
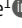











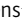
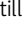


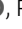






ARTICLE

# PU.1 enforces quiescence and limits hematopoietic stem cell expansion during inflammatory stress

James S. Chavez<sup>1</sup>, Jennifer L. Rabe<sup>1</sup>, Dirk Loeffler<sup>2</sup>, Kelly C. Higa<sup>3</sup>, Giovanni Hernandez<sup>1</sup>, Taylor S. Mills<sup>1,8</sup>, Nouraz Ahmed<sup>2</sup>, Rachel L. Gessner<sup>1</sup>, Zhonghe Ke<sup>1</sup>, Beau M. Idler<sup>1</sup>, Katia E. Niño<sup>1</sup>, Hyunmin Kim<sup>4</sup>, Jason R. Myers<sup>5</sup>, Brett M. Stevens<sup>1</sup>, Pavel Davizon-Castillo<sup>9</sup>, Craig T. Jordan<sup>1</sup>, Hideaki Nakajima<sup>6</sup>, John Ashton<sup>5</sup>, Robert S. Welner<sup>7</sup>, Timm Schroeder<sup>2</sup>, James DeGregori<sup>1,3,8,9</sup>, and Eric M. Pietras<sup>1,8</sup>

**Hematopoietic stem cells (HSCs) are capable of entering the cell cycle to replenish the blood system in response to inflammatory cues; however, excessive proliferation in response to chronic inflammation can lead to either HSC attrition or expansion. The mechanism(s) that limit HSC proliferation and expansion triggered by inflammatory signals are poorly defined. Here, we show that long-term HSCs (HSC<sup>L</sup>) rapidly repress protein synthesis and cell cycle genes following treatment with the proinflammatory cytokine interleukin (IL)-1. This gene program is associated with activation of the transcription factor PU.1 and direct PU.1 binding at repressed target genes. Notably, PU.1 is required to repress cell cycle and protein synthesis genes, and IL-1 exposure triggers aberrant protein synthesis and cell cycle activity in PU.1-deficient HSCs. These features are associated with expansion of phenotypic PU.1-deficient HSCs. Thus, we identify a PU.1-dependent mechanism triggered by innate immune stimulation that limits HSC proliferation and pool size. These findings provide insight into how HSCs maintain homeostasis during inflammatory stress.**

## Introduction

Hematopoietic stem cell (HSC) quiescence promotes lifelong blood regeneration and is controlled by a complex regulatory network, including cell-intrinsic transcription factors and epigenetic modifiers (Pietras et al., 2011), organelle homeostasis mechanisms (Hinge et al., 2020; Liang et al., 2020), and signals generated from the bone marrow (BM) niche (Morrison and Scadden, 2014). At least some portion of the HSC pool can be briefly forced out of quiescence to facilitate blood system regeneration by stressors such as infection (Prendergast and Essers, 2014), chronic stress (Heidt et al., 2014), and myeloablative injury (Harrison and Lerner, 1991), demonstrating that HSCs can replenish cells lost to disruptions in BM homeostasis (King and Goodell, 2011). However, tight regulation of cell cycle activity is crucial for maintaining the long-term functional integrity of the HSC pool (Matsumoto et al., 2011; Pietras et al., 2011). This is particularly true under inflammatory stress conditions, where increased proliferative activity can lead to functional attrition and/or aberrant expansion of the HSC

compartment, including in the contexts of chronic infection and/or genetic mutation associated with BM failure and myeloid oncogenesis (Essers et al., 2009; King et al., 2011; Matattal et al., 2016; Pietras, 2017; Pietras et al., 2014; Rodríguez et al., 2021; Takizawa et al., 2017; Walter et al., 2015; Zambetti et al., 2016; Zhang et al., 2016). Highly enriched HSC fractions can limit proliferative activity and maintain long-term engraftment capacity even under a variety of inflammatory stress conditions (Bujanover et al., 2018; Hernandez et al., 2020; Pietras et al., 2014; Pietras et al., 2016; Rabe et al., 2020; Wilson et al., 2008; Zhao et al., 2019), implying the existence of mechanism(s) that prevent excessive HSC cell cycle entry.

HSC can directly respond to pathogens and physiological danger signals via direct sensing (Takizawa et al., 2017) and/or paracrine proinflammatory cytokines produced by damaged and/or infected cells, such as IFNs (Ehninger et al., 2014; Essers et al., 2009; Matattal et al., 2016), G-CSF (Schuettpelez et al., 2014), TNF (Etzrodt et al., 2019; Yamashita and Passegué,

<sup>1</sup>Division of Hematology, University of Colorado Anschutz Medical Campus, Aurora, CO; <sup>2</sup>Department of Biosystems Science and Engineering, Eidgenössische Technische Hochschule Zurich, Basel, Switzerland; <sup>3</sup>Department of Biochemistry and Molecular Genetics, University of Colorado Anschutz Medical Campus, Aurora, CO; <sup>4</sup>Division of Medical Oncology, University of Colorado Anschutz Medical Campus, Aurora, CO; <sup>5</sup>Genomics Research Center, University of Rochester, Rochester, NY; <sup>6</sup>Department of Stem Cell and Immune Regulation, Yokohama City University School of Medicine, Yokohama, Japan; <sup>7</sup>Division of Hematology, Department of Medicine, University of Alabama at Birmingham, Birmingham, AL; <sup>8</sup>Department of Immunology and Microbiology, University of Colorado Anschutz Medical Campus, Aurora, CO; <sup>9</sup>Department of Pediatrics, University of Colorado Anschutz Medical Campus, Aurora, CO.

Correspondence to Eric M. Pietras: [eric.pietras@CUAnschutz.edu](mailto:eric.pietras@CUAnschutz.edu).

© 2021 Chavez et al. This article is distributed under the terms of an Attribution-Noncommercial-Share Alike-No Mirror Sites license for the first six months after the publication date (see <http://www.rupress.org/terms/>). After six months it is available under a Creative Commons License (Attribution-Noncommercial-Share Alike 4.0 International license, as described at <https://creativecommons.org/licenses/by-nc-sa/4.0/>).

2019), and IL-1 (Hemmati et al., 2019; Weisser et al., 2016). IL-1 consists of two cytokines (IL-1 $\alpha$  and IL-1 $\beta$ ) with different expression patterns that share a common receptor complex and elicit similar responses (Dinarelli, 2018). IL-1 is produced in response to a wide variety of physiological stress conditions, including aging; chronic inflammatory disease; myeloablative treatments, such as radiation and/or chemotherapy; obesity; and cellular senescence (Dinarelli, 2018; Laberge et al., 2015). It may also contribute to hematological malignancy and is highly expressed in cells from patients with myelodysplastic syndrome (MDS), myeloproliferative neoplasia, and acute myelogenous leukemia (Ågerstam et al., 2016; Barreyro et al., 2018; Carey et al., 2017; Ezaki et al., 1995; Zhang et al., 2016). Previous work from our group demonstrates that acute IL-1 exposure drives myeloid cell overproduction in vivo via precocious activation of the master myeloid transcription factor PU.1 (Pietras et al., 2016) in HSC. Interestingly, this effect is transient, as HSCs reenter quiescence following chronic exposure to IL-1. These findings imply the existence of a braking mechanism that limits HSC cell cycle entry in response to chronic inflammatory stress (Pietras et al., 2016; Rabe et al., 2020).

We recently found that quiescent HSCs downregulate numerous protein synthesis and cell proliferation genes in a mouse model of chronic rheumatoid arthritis (Hernandez et al., 2020). Interestingly, activation of this gene program relies, at least in part, on IL-1 signaling (Hernandez et al., 2020). In the present study, we further explore the relevance of this gene program to HSC function during chronic inflammation using a mouse model of chronic IL-1 stimulation (Pietras et al., 2016). We show that IL-1 signaling is sufficient to rapidly induce repression of a broad set of cell cycle and protein synthesis genes in HSCs, in turn limiting cell cycle activity. We find that repression of these genes in HSCs is associated with PU.1 expression, and chromatin immunoprecipitation sequencing (ChIP-seq) analysis shows that PU.1 directly binds these target genes. Strikingly, PU.1 deficiency leads to derepression of cell cycle and protein synthesis genes, licensing HSCs to increase protein synthesis activity and enter the cell cycle in response to IL-1 stimulation. Together, these data support a model in which PU.1 enforces HSC quiescence in response to inflammatory stress by limiting protein synthesis and cell cycle activity, thereby preventing aberrant expansion of the HSC pool.

## Results

### Chronic IL-1 induces repression of cell cycle and protein synthesis genes in long-term HSCs (HSC<sup>LT</sup>)

We previously found that HSCs maintain a largely quiescent state during chronic inflammatory stress driven by IL-1 and chronic inflammatory arthritis (Hernandez et al., 2020; Pietras, 2017; Pietras et al., 2014; Rabe et al., 2020). To address the mechanism(s), we analyzed gene expression by RNA sequencing (RNA-seq) in the HSC-enriched SLAM (signaling lymphocytic activation molecule) fraction (SLAM cells; LSK/Flk2<sup>-</sup>CD48<sup>-</sup>CD150<sup>+</sup>) isolated from the BM of mice treated with or without IL-1 $\beta$  for 20 d to model chronic inflammatory stress (Fig. 1 A; Pietras et al., 2016; Rabe et al., 2020). We found >1,400 differentially expressed genes

(DEGs;  $P_{\text{adj}} < 0.05$ ; Fig. 1 B and Table S1). Gene ontology (GO) analysis identified cell activation, immune response, leukocyte adhesion, and defense response gene programs among upregulated DEGs (Fig. S1 A and Table S2). Using a custom Fluidigm quantitative RT-PCR (qRT-PCR) array, we validated increased expression of key genes in these pathways, including *Itgam* (Mac-1), *Cdk6*, *Flt3*, *Il1r1*, and *Pdgfrb* (Fig. S1 B). Strikingly, downregulated DEGs were enriched for ribosome biogenesis, rRNA processing, transfer RNA processing, and translation GO categories (Fig. 1 C and Table S2), while Ingenuity Pathway Analysis (IPA) and Gene Set Enrichment Analysis (GSEA) likewise identified multiple cell proliferation and mRNA translation pathways inhibited by IL-1 (Fig. 1, D and E; and Table S2), which were likewise validated by qRT-PCR (Fig. S1 C). These data were strikingly reminiscent of *Myc* pathway downregulation we observed in SLAM cells from mice with collagen-induced arthritis (CIA; Hernandez et al., 2020), and comparison with our prior GSEA analyses of SLAM cells from CIA mice revealed significant overlap in translation and ribosome gene signature enrichment between datasets (Fig. S1 D), suggesting repression of translation pathways in HSCs is not exclusively a property of in vivo IL-1 stimulation and can be observed in physiological models of chronic inflammatory disease.

We previously showed that HSC<sup>LT</sup>-enriched SLAM cells (defined as LSK/Flk2<sup>-</sup>CD48<sup>-</sup>CD150<sup>+</sup>CD34<sup>-</sup>EPCR<sup>+</sup>; Fig. S1 E) overlap phenotypically with deeply quiescent CD49b<sup>lo</sup> reserve HSCs (Zhao et al., 2019) and remain almost exclusively in a quiescent (G<sub>0</sub>) cell cycle state, despite chronic IL-1 exposure (Rabe et al., 2020). Cell cycle and protein synthesis genes were likewise repressed in chronic IL-1-exposed HSC<sup>LT</sup> (Fig. 1 F), and we confirmed reduced *Myc* expression in HSCs by intracellular flow cytometry staining (Fig. 1 G and Fig. S1 F). *Myc* levels in phenotypic MPP4 (LSK/Flk2<sup>+</sup>) were not significantly impacted by chronic IL-1, suggesting that not all progenitor cells repress *Myc* to the same extent in response to IL-1 (Fig. S1 F). Since chronic IL-1 exposure reduced expression of protein synthesis genes, we also measured the impact of chronic IL-1 exposure on protein synthesis rates in HSC<sup>LT</sup> by in vivo puromycin (puro) incorporation assays (Fig. 1 H). Consistent with prior work (Signer et al., 2014), puro incorporation rates in HSC<sup>LT</sup>, SLAM cells, and MPP4 were all similar (Fig. S1 G), and chronic IL-1 exposure did not impact the HSC<sup>LT</sup> protein synthesis rate (Fig. 1 H and Fig. S1 G). Lastly, we confirmed our prior published findings that HSC<sup>LT</sup> were quiescent after chronic IL-1 exposure (Fig. 1, I–K; Rabe et al., 2020). Taken together, these data suggest that repression of cell cycle and protein synthesis genes is associated with homeostatic protein synthesis and cell cycle activity in HSC<sup>LT</sup> during chronic inflammatory stress.

### IL-1-induced gene repression is rapid and independent of HSC<sup>LT</sup> divisional history

Since IL-1-repressed genes primarily appear to regulate mechanisms associated with cell proliferation, we first assessed whether this gene program was also activated in response to acute IL-1 exposure (a single IL-1 injection; Fig. 2 A). Consistent with prior investigations, we found that a single injection of IL-1 rapidly induced robust cell cycle activity in the SLAM compartment (Fig. 2, B and C). Concurrently, we observed a

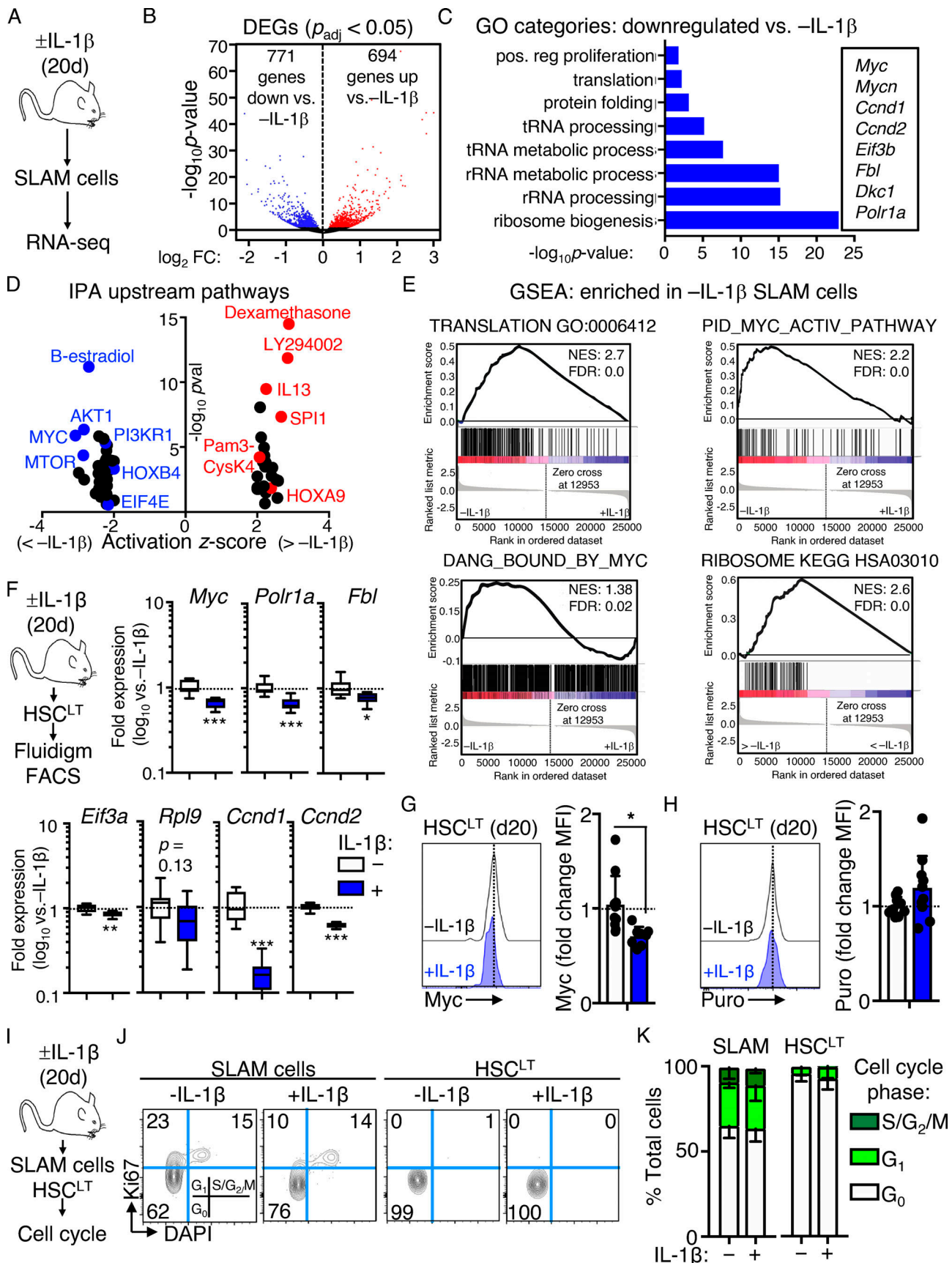


Figure 1. **Chronic IL-1 induces repression of cell cycle and protein synthesis genes.** (A) Experimental design for RNA-seq studies ( $n = 4-7$  pools of SLAM cells from mice treated for 20 d ±IL-1β). Pools were generated from three independent cohorts of mice. (B) Volcano plot of DEGs ( $P_{adj} \leq 0.05$ ) in IL-1-exposed



SLAM cells (LSK/Flk2<sup>-</sup>/CD48<sup>-</sup>/CD150<sup>+</sup>) from A showing log<sub>2</sub> fold change (FC) versus -log<sub>10</sub> P value significance. See also Table S1. **(C)** GO category enrichment of downregulated DEGs in IL-1-exposed SLAM cells from A, expressed as -log<sub>10</sub> P value. See also Table S2. **(D)** IPA showing enriched upstream regulators of DEGs in IL-1-exposed SLAM cells from A. See also Table S3. **(E)** GSEA analysis of significantly downregulated DEGs. GSEA plots show negative enrichment of translation and Myc pathway genes in IL-1-exposed SLAM cells from A. See also Table S4. **(F)** Experimental design for Fluidigm qRT-PCR analyses and intracellular FACS staining of HSC<sup>LT</sup> (LSK/Flk2<sup>-</sup>/CD48<sup>-</sup>/CD150<sup>+</sup>/CD34<sup>-</sup>/EPCR<sup>+</sup>) from mice treated for 20 d with or without IL-1β (left), and quantification by Fluidigm qRT-PCR array of cell cycle and protein synthesis gene expression in HSC<sup>LT</sup> (*n* = 8/group). Data are expressed as log<sub>10</sub> fold expression versus -IL-1β. Box represents upper and lower quartiles with line representing median value. Whiskers represent minimum and maximum values. Data are representative of two independent experiments. **(G)** Intracellular flow cytometry analysis of Myc protein levels in HSC<sup>LT</sup> (*n* = 10 -IL-1β; 8 +IL-1β). Data are expressed as fold change of MFI versus -IL-1β. Individual values are shown with bars representing mean values. Data are compiled from three independent experiments. **(H)** Intracellular flow cytometry analysis of puromycin incorporation in HSC<sup>LT</sup> (*n* = 9 -IL-1β; 10 +IL-1β). Data are expressed as fold change of MFI versus -IL-1β. Individual values are shown with bars representing mean values. Data are compiled from three independent experiments. **(I)** Experimental design for cell cycle analyses of SLAM cells and HSC<sup>LT</sup> from mice treated for 20 d with or without IL-1. **(J)** Representative flow cytometry plots showing cell cycle distribution in SLAM cells and HSC<sup>LT</sup> from I. **(K)** Quantification of cell cycle phase distribution in SLAM cells and HSC<sup>LT</sup> from I (*n* = 5/group). Data are representative of three independent experiments. \*, *P* < 0.05; \*\*, *P* < 0.01; \*\*\*, *P* < 0.001 by Mann-Whitney *U* test or ANOVA with Tukey's test in K. Error bars represent SD. See also Fig. S1.

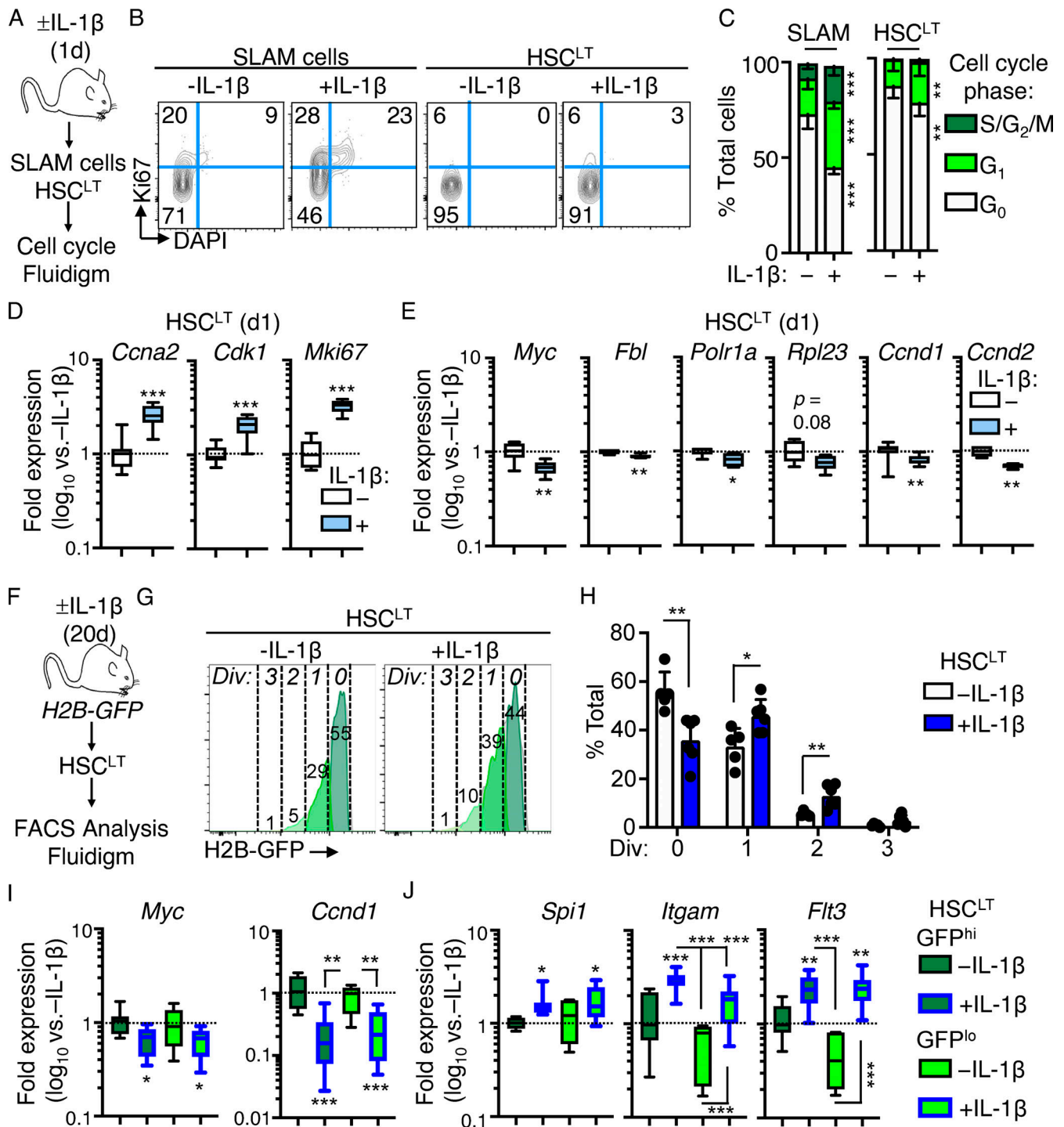
limited, though significant, induction of cell cycle activity in phenotypic HSC<sup>LT</sup> after acute IL-1 exposure (Fig. 2, B and C). Strikingly, Fluidigm analysis of HSC<sup>LT</sup> revealed that, while genes such as *Ccna2* and *Mki67* were upregulated, consistent with increased cell cycle activity in this compartment (Fig. 2 D), *Myc* and other protein synthesis genes downregulated under chronic IL-1 conditions were rapidly repressed even under acute IL-1 conditions (Fig. 2 E). Given this finding, we next asked whether downregulation of these genes was triggered exclusively in HSC<sup>LT</sup> that had entered the cell cycle following IL-1 exposure. Hence, we used *Colla-TetO::H2B-GFP* mice (Foudi et al., 2009) to distinguish undivided phenotypic HSC<sup>LT</sup> from phenotypic HSC<sup>LT</sup> with accumulated divisional history following chronic IL-1 exposure (Fig. 2 F). We induced H2B-GFP transgene for 2 wk with doxycycline chow (Sawén et al., 2016) followed by a 1-wk rest and subsequent chase period of 20 d with or without IL-1 injection. Consistent with our cell cycle analysis showing acute induction of HSC<sup>LT</sup> cell cycle activity, we observed an increase in H2B-GFP dilution in phenotypic HSC<sup>LT</sup> from IL-1-treated mice (Fig. 2, G and H). These data were indicative of roughly a single extra division in some, but not all, HSC<sup>LT</sup>. We therefore assessed whether IL-1 repressed *Myc* and *Ccnd1* exclusively in HSC<sup>LT</sup> that had divided or vice versa. Notably, qRT-PCR analysis of GFP<sup>hi</sup> (undivided) versus GFP<sup>lo</sup> (divided) HSC<sup>LT</sup> (Fig. S1, H and I) showed that *Myc* and *Ccnd1* were repressed equally in HSC<sup>LT</sup> regardless of divisional history (Fig. 2 I). Likewise, both GFP<sup>hi</sup> and GFP<sup>lo</sup> HSC<sup>LT</sup> subsets also upregulated IL-1 target genes, including *Spil* (*PU.1*), *Itgam*, and *Flt3* equally, suggesting proliferative history did not impact sensitivity to IL-1 (Fig. 2 I). Taken together, our data indicate that IL-1 rapidly induces repression of *Myc* and other cell cycle and protein synthesis genes in a manner independent of divisional history.

### IL-1-induced gene repression is associated with increased PU.1 levels

To investigate how IL-1 represses cell cycle and protein synthesis genes in HSC<sup>LT</sup>, we reanalyzed our IPA data and noticed that it had identified SPI1 (*PU.1*) pathway activation in IL-1-exposed SLAM cells (Fig. 1 D), consistent with our prior published findings (Etzrodt et al., 2019; Pietras et al., 2016; Rabe et al., 2020). Interestingly, *PU.1* can also restrict proliferation in hematopoietic stem and progenitor cells (HSPCs), likely a mechanism to

promote *PU.1* accumulation during myeloid differentiation (Fukuchi et al., 2008; Kueh et al., 2013). We reasoned this mechanism could also serve to restrict HSC activation by IL-1. To establish a relationship between *PU.1* and IL-1-mediated repression of cell cycle and protein synthesis genes, we first compared our RNA-seq dataset with publicly available datasets in which *PU.1* was overexpressed in thymocytes (Hosokawa et al., 2018; Gene Expression Omnibus [GEO] accession no. GSE93755) and in which *Myc* and *Mycn* were conditionally deleted in HSCs, leading to reduced proliferative activity (Laurenti et al., 2008; GEO accession no. GSE12467). GSEA analysis revealed that cell cycle and protein synthesis genes repressed in these datasets were likewise repressed in SLAM cells from IL-1-exposed mice (i.e., enriched in -IL-1 SLAM cells; Fig. 3 A). We also identified a common signature of cell cycle and protein synthesis genes, including *Myc* itself, repressed in all three RNA-seq datasets (Fig. 3 B and Table S3).

We then generated *PU.1-EYFP::GFP-Myc* dual-reporter mice using previously published *PU.1-EYFP* and *GFP-Myc* reporter mouse strains (Fig. 3 C; Hoppe et al., 2016; Huang et al., 2008; Kirstetter et al., 2006). As these reporters consist of fluorescent fusion proteins knocked into the endogenous loci, we could directly read out in the same cells the correlation between *PU.1* and *Myc* expression. We observed lineage-specific expression patterns of *PU.1* and *Myc* in HSPCs from these mice, with granulocyte-macrophage progenitors (LK/CD41<sup>-</sup>/FcgR<sup>+</sup>; Pronk et al., 2007) expressing high levels of *PU.1*, whereas phenotypic CFU-erythroid (LK/CD41<sup>-</sup>/FcgR<sup>-</sup>/CD150<sup>-</sup>/CD105<sup>+</sup>) expressed high *Myc* levels but low *PU.1* levels (Fig. S1, J and K). Consistent with our prior work, chronic IL-1 increased *PU.1* expression and the frequency of *PU.1*<sup>hi</sup> SLAM cells (Fig. 3, C and D; Pietras et al., 2016). Notably, *GFP-Myc* levels decreased significantly in *PU.1*<sup>hi</sup> SLAM cells following chronic IL-1 exposure (Fig. 3 E), which we independently validated by staining for *Myc* protein in *PU.1*<sup>hi</sup> HSC<sup>LT</sup> (Fig. S2, A and B). These data support a model in which IL-1-induced *PU.1* represses *Myc*. To assess whether increased *PU.1* expression was associated with repression of other genes identified by our RNA-seq study, we performed Fluidigm qRT-PCR analysis on *PU.1*<sup>hi</sup> and *PU.1*<sup>lo</sup> SLAM cells isolated from mice treated with or without IL-1 for 20 d (Fig. S2 A). Expectedly, *Spil* (*PU.1*) was further upregulated in *PU.1*<sup>hi</sup> SLAM cells by IL-1, whereas *Myc* and several cell cycle and protein synthesis genes repressed by IL-1 were specifically downregulated in *PU.1*<sup>hi</sup> SLAM cells (Fig. S2 C).



**Figure 2. IL-1-induced gene repression is rapid and independent of HSC<sup>LT</sup> divisional history.** (A) Experimental design for cell cycle analyses of SLAM cells and HSC<sup>LT</sup> from mice treated for 1 d with or without IL-1 $\beta$ . (B) Representative flow cytometry plots showing cell cycle distribution in SLAM cells and HSC<sup>LT</sup> from A. (C) Quantification of cell cycle phase distribution in SLAM cells and HSC<sup>LT</sup> from A ( $n = 10$ /group). Data are compiled from three independent experiments. (D) Quantification by Fluidigm qRT-PCR array of cell cycle gene expression in HSC<sup>LT</sup> from mice treated for 1 d with or without IL-1 $\beta$  ( $n = 8$ /group). Data are expressed as  $\log_{10}$  fold expression versus -IL-1 $\beta$ . Box represents upper and lower quartiles with line representing median value. Whiskers represent minimum and maximum values. Data are representative of two independent experiments. (E) Quantification of IL-1-repressed protein synthesis and cell cycle genes from Fluidigm qRT-PCR array in D. Data are representative of two independent experiments. (F) Experimental design for analysis of divisional history in HSC<sup>LT</sup> using H2B-GFP mice treated for 20 d with or without IL-1 $\beta$ . (G) Representative FACS plots showing analysis of HSC<sup>LT</sup> divisional history via GFP dilution from H2B-GFP mice treated for 20 d with or without IL-1 $\beta$ . (H) Quantification of divisional history of mice in F based on GFP dilution ( $n = 5-6$ /group). Data are compiled from two independent experiments. (I) Quantification by Fluidigm qRT-PCR array of IL-1-repressed genes in GFP<sup>hi</sup> and GFP<sup>lo</sup> HSC<sup>LT</sup> from H2B-GFP mice in F ( $n = 8$ /group). Data are expressed as  $\log_{10}$  fold expression versus -IL-1 $\beta$ . Box represents upper and lower quartiles with line representing median value. Whiskers represent minimum and maximum values. Data are representative of two independent experiments. (J) Quantification of IL-1 target genes from Fluidigm qRT-PCR array in I. Data are representative of two independent experiments. \*,  $P < 0.05$ ; \*\*,  $P < 0.01$ ; \*\*\*,  $P < 0.001$  by Mann-Whitney  $U$  test or ANOVA with Tukey's test in C, H, I, and J. Error bars represent SD. See also Fig. S1.

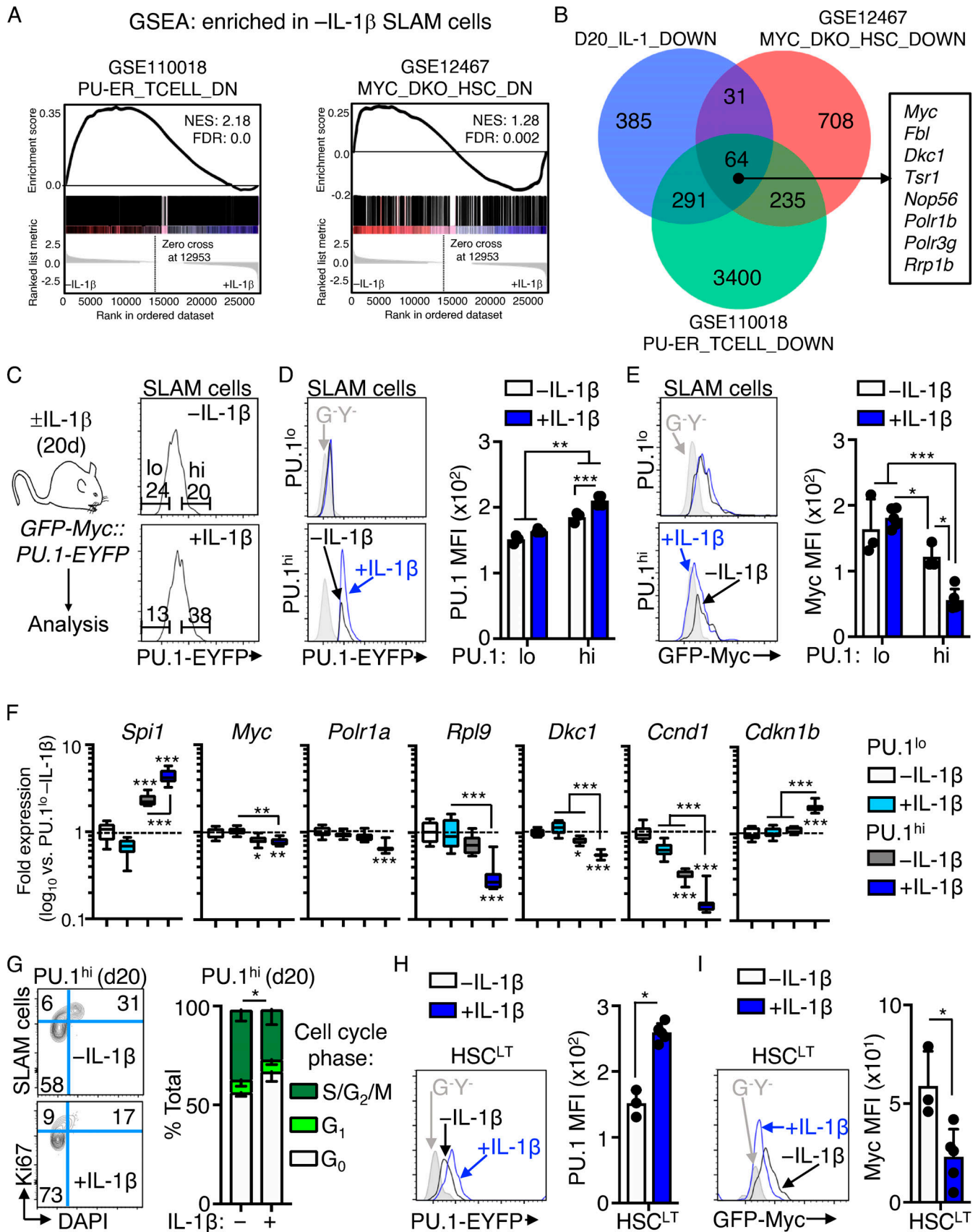


Figure 3. **IL-1-induced gene repression is associated with high PU.1 levels.** (A) GSEA enrichment of significantly downregulated genes in publicly available datasets versus RNA-seq analysis of SLAM cells from mice treated with or without  $IL-1\beta$  for 20 d. Data show downregulated genes as negatively enriched in



SLAM cells from mice treated for 20 d with or without IL-1 $\beta$ . See also Table S5. **(B)** Venn diagram showing intersections between gene sets in A. A partial list of common genes is depicted at the right of the diagram. See also Table S6 for complete list of genes. **(C)** Left: Experimental design for analysis of *PU.1-EYFP::GFP-Myc* mice treated with or without IL-1 $\beta$  for 20 d. Right: Representative FACS plots showing gating strategy to identify PU.1<sup>lo</sup> and PU.1<sup>hi</sup> SLAM cells based on PU.1-EYFP expression levels in these mice. **(D)** Representative FACS plots (left) and quantification (right) showing PU.1-EYFP expression levels in PU.1<sup>lo</sup> and PU.1<sup>hi</sup> SLAM cell fractions from C ( $n = 3$  -IL-1 $\beta$ ; 5 +IL-1 $\beta$ ). PU.1-EYFP negative control is shown in gray. Individual values are shown with bars representing mean values. Data are representative of two independent experiments. **(E)** Representative FACS plots (left) and quantification (right) showing GFP-Myc expression levels in PU.1<sup>lo</sup> and PU.1<sup>hi</sup> SLAM cell fractions from C ( $n = 3$  -IL-1 $\beta$ ; 5 +IL-1 $\beta$ ). GFP-Myc negative control is shown in gray. Individual values are shown with bars representing mean values. Data are representative of two independent experiments. **(F)** Quantification by Fluidigm qRT-PCR array of cell cycle and protein synthesis gene expression in PU.1<sup>hi</sup> and PU.1<sup>lo</sup> SLAM cells from mice treated with or without IL-1 $\beta$  for 20 d ( $n = 8$ /group). Data are expressed as log<sub>10</sub> fold expression versus -IL-1 $\beta$ . Box represents upper and lower quartiles with line representing median value. Whiskers represent minimum and maximum values. Data are representative of two independent experiments. **(G)** Representative FACS plots (left) and quantification (right) of cell cycle distribution in PU.1<sup>hi</sup> SLAM cells from mice treated with or without IL-1 $\beta$  for 20 d ( $n = 3$ /group) using Ki-67 and DAPI. Data are compiled from two independent experiments. **(H)** Representative FACS plots (left) and quantification (right) showing PU.1-EYFP expression levels in HSC<sup>LT</sup> from mice in C ( $n = 3$  -IL-1 $\beta$ ; 5 +IL-1 $\beta$ ). PU.1-EYFP negative control is shown in gray in FACS plots. Individual values are shown with bars representing mean values. Data are representative of two independent experiments. **(I)** Representative FACS plots (left) and quantification (right) showing GFP-Myc expression levels in PU.1<sup>lo</sup> and PU.1<sup>hi</sup> SLAM cell fractions from mice in C. GFP-Myc negative control is shown in gray in FACS plots. Individual values are shown with bars representing mean values. Data are representative of two independent experiments. \*,  $P < 0.05$ ; \*\*,  $P < 0.01$ ; \*\*\*,  $P < 0.001$  by Mann-Whitney  $U$  test or ANOVA with Tukey's test in D–G. Error bars represent SD. See also Figs. S1 and S2.

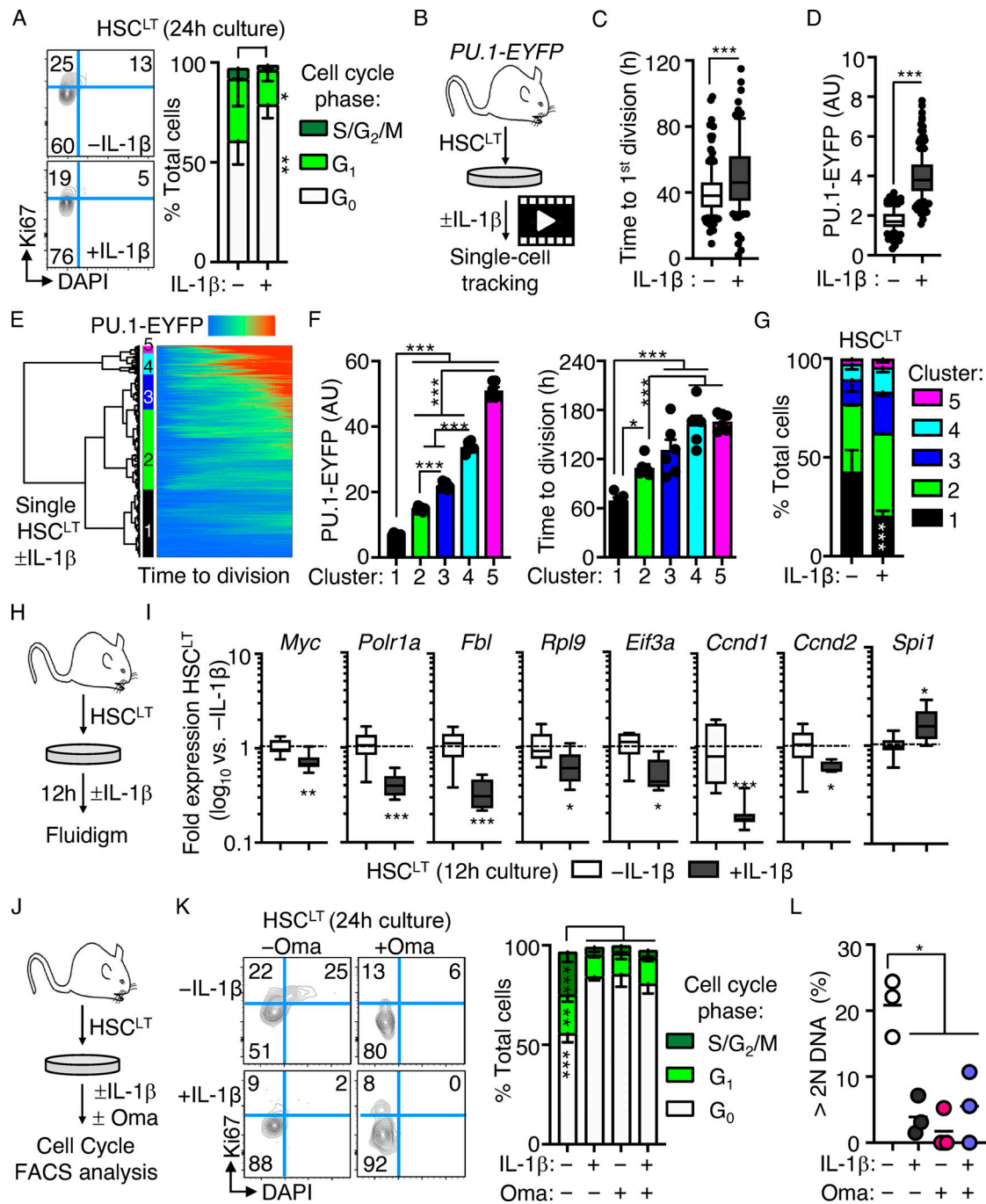
Likewise, known IL-1/PU.1 target genes, such as *Itgam*, *Flt3*, and *Iltr1*, were elevated in PU.1<sup>hi</sup> SLAM cells and further upregulated by IL-1 treatment (Fig. S2 C). Our data also showed that PU.1<sup>hi</sup> SLAM cells expressed lower levels of Mk/E genes like *Gata1* than PU.1<sup>lo</sup> SLAM cells, consistent with lineage-related anticorrelations between PU.1 and *Gata-1* (Fig. S2 D). Furthermore, IL-1 exposure enriched for HSC genes in PU.1<sup>hi</sup> SLAM cells (Fig. S2 E), suggesting that the frequency of HSC<sup>LT</sup> in the PU.1<sup>hi</sup> phenotypic gate increases following IL-1 exposure. Consistent with PU.1-mediated repression of cell cycle and protein synthesis genes, in vivo chronic IL-1 exposure decreased cell cycle activity in PU.1<sup>hi</sup> SLAM cells, whereas IL-1 triggered increased cell cycle activity in the PU.1<sup>lo</sup> SLAM fraction (Fig. 3 G and Fig. S2 F). To link all of these findings back to phenotypic HSC<sup>LT</sup> under chronic IL-1 conditions, we assessed PU.1-EYFP and Myc-GFP levels after 20 d of IL-1 treatment. As predicted by our data, phenotypic HSC<sup>LT</sup> expressed elevated levels of PU.1-EYFP, whereas GFP-Myc levels were reduced (Fig. 3, H and I). We observed a similar pattern of cell cycle activity and gene expression after acute (1 d) in vivo IL-1 stimulation, with relatively limited induction of cell cycle activity in PU.1<sup>hi</sup> SLAM cells that coincided with repression of genes, including *Myc*, *Cnd1*, and *Rpl9* (Fig. S2, G and H), and increased expression of PU.1-EYFP in HSC<sup>LT</sup> (Fig. S2 I). Altogether, our data show that elevated PU.1 expression is associated with repression of cell cycle and protein synthesis genes in SLAM cells and HSC<sup>LT</sup>.

#### Direct IL-1 stimulation in vitro induces PU.1 and restricts HSC<sup>LT</sup> cell cycle entry

We next assessed whether IL-1 could directly restrict cell cycle activity following IL-1 stimulation of HSC<sup>LT</sup> in vitro. Notably, cell cycle entry was delayed in HSC<sup>LT</sup> cultured for 24 h with IL-1 (Fig. 4 A). To address the link with PU.1, we next analyzed HSC<sup>LT</sup> division kinetics with or without IL-1 using live single-cell imaging of cultured *PU.1-EYFP* HSC<sup>LT</sup> (Fig. 4 B). Consistent with our cell cycle analyses, IL-1 significantly delayed—but did not halt—the initial cell division of cultured HSC<sup>LT</sup> (Fig. 4 C), consistent with our prior single-cell tracking studies in SLAM cells (Pietras et al., 2016). PU.1-EYFP levels were also rapidly and

significantly increased in HSC<sup>LT</sup> cultured with IL-1 before the first cell division, also consistent with previous observations for TNF (Fig. 4 D; Etzrodt et al., 2019). To more clearly delineate the relationship between PU.1 level and division kinetics, we performed unsupervised hierarchical clustering analysis of PU.1-EYFP expression patterns across time from first observation until cell division for all our tracked HSC<sup>LT</sup> with or without IL-1 (Fig. 4 E). Hierarchical clustering analysis identified five clusters based on PU.1-EYFP reporter expression dynamics in individual HSC<sup>LT</sup> (Fig. 4, E and F), with cluster 1 representing cells with low or nearly absent PU.1-EYFP reporter activity. Notably, HSC<sup>LT</sup> with low PU.1 expression levels (cluster 1) had significantly shorter division kinetics than HSC<sup>LT</sup> with higher PU.1 expression levels (clusters 2–5). To address the impact of IL-1, we next separated cells by treatment condition and analyzed the distribution of clusters in each. Strikingly, IL-1 treatment significantly reduced the number of rapidly dividing PU.1<sup>lo</sup> HSCs in cluster 1, with these cells instead distributing into clusters 2–5 (Fig. 4 G). We also assessed whether increased PU.1 expression was sufficient to delay HSC<sup>LT</sup> cell division by analyzing the division kinetics of transgenic *PU.1-ERT* HSC<sup>LT</sup>, which activate exogenous PU.1 upon induction with tamoxifen (4-OHT; Fukuchi et al., 2008). As expected, PU.1 activation enforced a delay in HSC<sup>LT</sup> division kinetics similar to the effects of IL-1 (Fig. S3 A). Taken together, these data indicate a positive correlation between PU.1 levels and cell cycle progression.

IL-1 treatment also rapidly repressed cell cycle and protein synthesis genes in HSC<sup>LT</sup> after 12 h in culture (Fig. 4, H and I), with a corresponding increase in *Spi1*. Given the broad down-regulation of protein synthesis genes, we assessed whether reduced protein synthesis is sufficient to limit HSC<sup>LT</sup> cell cycle entry. We thus compared the impact of IL-1 versus omacetaxine (Oma), which binds the ribosomal A-site and inhibits protein synthesis (Gandhi et al., 2014), on HSC<sup>LT</sup> cell cycle entry (Fig. 4 J). Like IL-1, Oma effectively limited HSC cell cycle entry and reduced total Ki-67 protein expression (Fig. 4 K). Since reduced Ki-67 levels may be related to translation inhibition and not cell cycle changes, we independently read out cell cycle progression based on the frequency of cells with >2N DNA



**Figure 4. Direct IL-1 stimulation in vitro induces PU.1 and restricts HSC<sup>LT</sup> cell cycle entry.** (A) Representative FACS plots (left) and quantification (right) of cell cycle distribution in HSC<sup>LT</sup> cultured for 24 h with or without IL-1 $\beta$  ( $n = 6$ /group). Data are compiled from three independent experiments. (B) Experimental design for single-cell tracking studies of PU.1-EYFP HSC<sup>LT</sup> cultured with or without IL-1 $\beta$ . Time to first cell division was tracked via microscopy. (C) Graph showing kinetics of first cell division in HSC<sup>LT</sup> from B ( $n = 194$  -IL-1 $\beta$ ; 139 IL-1 $\beta$ ). Data are compiled from three independent experiments. (D) PU.1-EYFP levels in HSC<sup>LT</sup> before first cell division ( $n = 137$  -IL-1 $\beta$ ; 192 +IL-1 $\beta$ ). Data are compiled from three independent experiments. Box shows upper and lower quartiles with line showing median value, and whiskers upper and lower 10th percentile and individual dots represent outliers. (E) Hierarchical clustering analysis of PU.1-EYFP expression over time from the start of observation until the first division in PU.1-EYFP HSC<sup>LT</sup> cultured with or without IL-1 (Euclidean distance with Ward linkage;  $n = 557$  -IL-1 $\beta$ ; 489 +IL-1 $\beta$ ). Data are compiled from three independent experiments. (F) Quantification of PU.1-EYFP level (as arbitrary units [AU]; left) and time to division (right) of HSC<sup>LT</sup> cultured with or without IL-1 $\beta$  in E. Individual values (representing means from cells cultured either with or without IL-1 $\beta$  in an experiment) are shown with bars representing mean values ( $n = 6$ ). Data are compiled from three independent experiments. (G) Distribution of HSC<sup>LT</sup> from E in different clusters based on culture with or without IL-1 $\beta$ . Data are compiled from three independent experiments. (H) Experimental design for Fluidigm qRT-PCR array analysis of HSC<sup>LT</sup> cultured with or without IL-1 $\beta$  for 12 h. (I) Quantification by Fluidigm qRT-PCR array of cell cycle and protein synthesis gene expression in HSC<sup>LT</sup> from F ( $n = 8$ /group). Data are expressed as log<sub>10</sub> fold expression versus -IL-1 $\beta$ . Box represents upper and lower quartiles with line representing median value. Whiskers represent minimum and maximum values. Data are representative of two independent experiments. (J) Experimental design for cell cycle analysis of HSC<sup>LT</sup> cultured with or without IL-1 $\beta$  and with or without 100 nM Oma for 24 h. (K)



Representative FACS plots (left) and quantification (right) of cell cycle distribution in HSC<sup>LT</sup> from H ( $n = 3/\text{group}$ ). Data are from one experiment. (L) Proportion of HSC<sup>LT</sup> with >2N DAPI signal from H. Individual values are shown with means (horizontal line). \*,  $P < 0.05$ ; \*\*,  $P < 0.01$ ; \*\*\*,  $P < 0.001$  by Mann-Whitney  $U$  test or one-way ANOVA with Tukey's test in F, G, K, and L. Error bars represent SD. See also Fig. S3.

content (i.e., S/G<sub>2</sub>/M phases) based on DAPI alone. We observed a significant reduction in IL-1 and/or Oma-treated HSC<sup>LT</sup> in S phase or beyond, consistent with slowed cell cycle activity (Fig. 4 L). Oma and IL-1 also reduced the forward scatter (FSC) profile of cultured HSCs, consistent with previous observations correlating cell size and biosynthetic activity (Fig. S3 B; Iritani and Eisenman, 1999; Scognamiglio et al., 2016). Collectively, these data indicate that IL-1 directly and rapidly represses cell cycle and protein synthesis genes, thereby limiting HSC<sup>LT</sup> cell cycle entry in vitro.

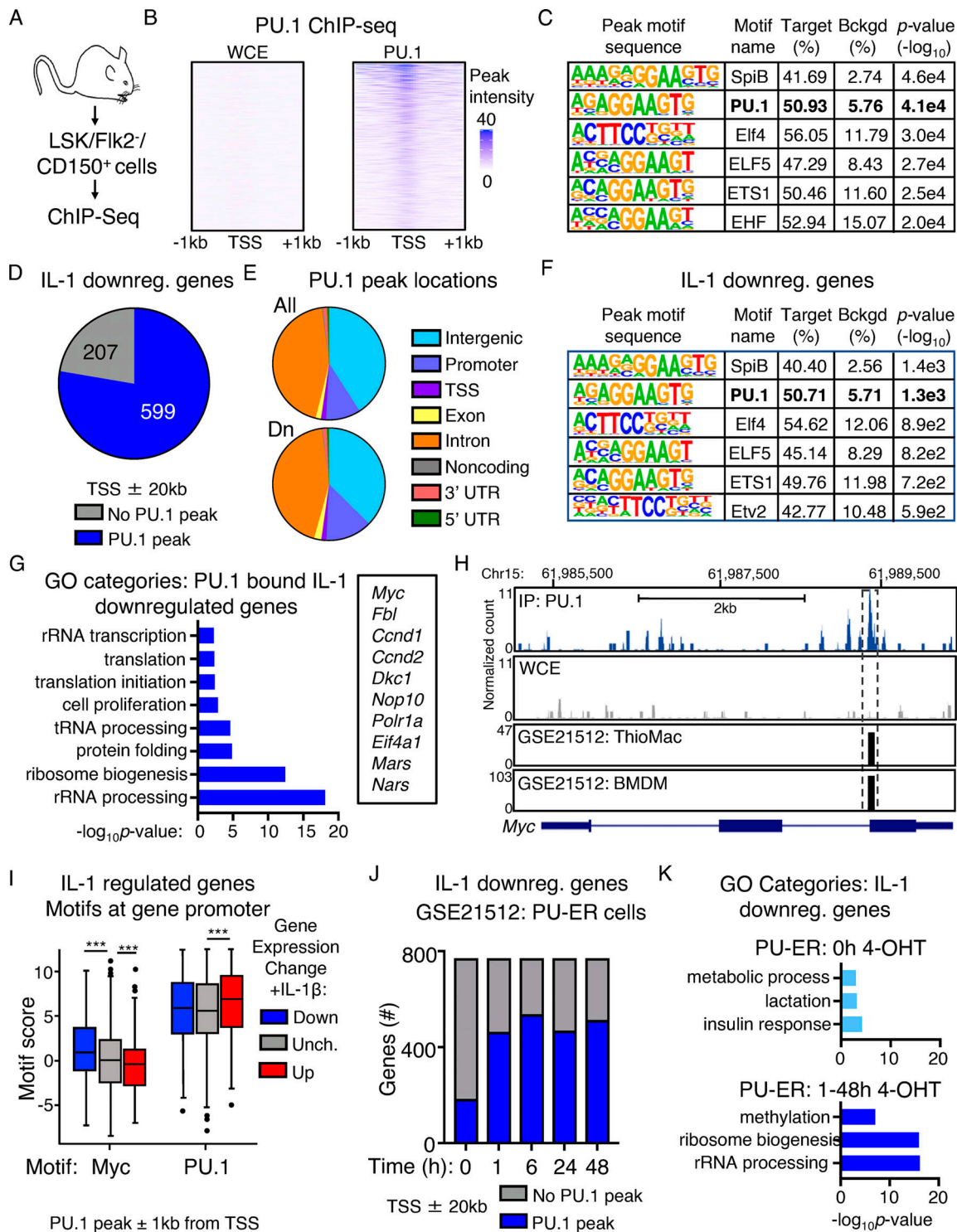
### PU.1 directly binds cell cycle and protein synthesis genes repressed by IL-1

Given the association between high PU.1 levels and IL-1-induced repression of translation and cell cycle genes, we asked whether PU.1 directly interacts with these genes. We therefore analyzed genome-wide PU.1 binding using ChIP-seq analysis of HSC-enriched LSK/Flk2<sup>-</sup>/CD150<sup>+</sup> cells (Fig. 5 A). Relative to whole-cell extract (WCE) controls, we identified 52,127 unique and specific PU.1 peaks located throughout the genome, with significant enrichment at 5'-GGAA-3'-containing consensus motifs within 200 bp of the peak sites (Fig. 5, B and C; and Table S4). Notably, the vast majority of IL-1 DEGs (586/694 IL-1 up; 599/771 IL-1 down) had PU.1 peaks located predominantly in intronic or intergenic regions within  $\pm 20$  kb of the gene transcription start site (TSS), likewise within 200 bp of 5'-GGAA-3'-containing consensus motifs (Fig. 5, D-F; Fig. S4, A-C; and Table S4). GO analysis of IL-1-repressed genes associated with PU.1 ChIP-seq peaks revealed expected enrichment for rRNA processing, cell proliferation, and translation categories (Fig. 5 G and Table S5). We next analyzed PU.1 peaks associated with the *Myc* gene and found several located within  $\pm 20$  kb of the TSS itself, including a peak located within the gene body near the junction of intron 2/exon 3 (Fig. 5 H) and several located in the 3' intergenic space (Table S4). The intronic *Myc* peak was also present in two independent published macrophage datasets (Heinz et al., 2010; GEO accession no. GSE21512). Indeed, PU.1 peaks identified in our ChIP-seq dataset corresponded closely with peaks in these two datasets (Table S4). Conversely, IL-1-induced genes with PU.1 peaks were enriched for cell adhesion, immune response, and other expected gene categories (Fig. S4 D and Table S5), including the PU.1 target gene *Itgam*, which contained several peaks located both in the gene body as well as in the 5' intergenic region, including a site near the TSS/promoter as previously characterized and a major peak that may represent an enhancer site (Fig. S4 E). Interestingly, we also noted that a subset of IL-1-downregulated genes with PU.1 were also significantly enriched for *Myc* motifs within 1 kb of their TSS relative to upregulated or unchanged genes (Fig. 5 I and Table S4), further underscoring the negative regulatory relationship between PU.1 and *Myc* target genes. We also used an in vitro luciferase reporter assay to demonstrate that PU.1 can

directly repress activity of the human *Myc* promoter (Fig. S4 F), in line with prior studies indicating that PU.1 can be recruited to the *Myc* promoter in complex with histone deacetylase proteins (Kihara-Negishi et al., 2001). To further characterize the dynamics of PU.1 interactions with IL-1 target genes, we reanalyzed published ChIP-seq data (Heinz et al., 2010; GEO accession no. GSE21512) generated in *PU.1*<sup>-/-</sup> fetal liver hematopoietic progenitor cells expressing a 4-OHT-inducible *PU.1* transgene (PU-ER cells) at different time points postinduction (Heinz et al., 2010). These cells constitutively express a low level of PU.1 from the transgene, with 4-OHT rapidly inducing PU.1 protein activation (Walsh et al., 2002). We found that activation of the *PU.1* transgene leads to reduced *Myc* expression and a small but significant cell cycle delay in PU-ER cells, suggesting that, despite the difference in cell type and origin, the response to PU.1 expression in this system resembles key features of IL-1-treated HSC<sup>LT</sup> (Fig. S4, G and H). In the PU-ER cell ChIP-seq dataset, a small fraction (177 total) of IL-1-repressed genes were constitutively bound by low levels of PU.1 present in the absence of 4-OHT (0 h). Interestingly, those genes were unrelated to cell cycle or protein synthesis (Fig. 5, J and K). The number of IL-1-repressed genes bound by PU.1 increased significantly and rapidly with 4-OHT treatment, with top GO categories of these genes now including ribosome biogenesis and rRNA processing (Fig. 5, J and K). We observed a similar pattern of expression for IL-1-upregulated genes, though in this case inflammatory response genes were already bound by PU.1 at 0 h (Fig. S4, J and K; and Table S5) and transgene-inducible peaks centered around cell adhesion and mitotic cell division gene categories (Fig. S4 K), with the latter centered around genes required for late cell cycle stages rather than quiescence exit. Taken together, these data support a model in which PU.1 represses gene expression by directly binding a broad set of cell cycle and protein synthesis genes. They also suggest that, at reduced levels, PU.1 does not bind the majority of IL-1-repressed cell cycle and protein synthesis genes.

### PU.1-deficient HSC<sup>LT</sup> overexpress cell cycle and protein synthesis genes

To further explore the impact of reduced PU.1 expression on HSC<sup>LT</sup> function, we analyzed *PU.1*<sup>KI/KI</sup> mice, which express ~30% of normal PU.1 levels in SLAM cells due to a deactivating point mutation knocked into the 14-kb upstream *Sp1* autoregulatory binding motif (Staber et al., 2013). As SLAM cells from these mice exhibit derepression of cell cycle genes, including *Ccnd1*, *E2f*, and *Cdkl*, we first compared our RNA-seq data to published gene expression microarray data from *PU.1*<sup>+/+</sup> and *PU.1*<sup>KI/KI</sup> SLAM cells (Staber et al., 2013; GEO accession no. GSE33031). Expectedly, several cell cycle and protein synthesis genes repressed by IL-1, including *Myc*, were significantly upregulated in *PU.1*<sup>KI/KI</sup> SLAM cells (Fig. 6 A). We therefore assessed gene expression in HSC<sup>LT</sup> from *PU.1*<sup>KI/KI</sup> mice and *PU.1*<sup>+/+</sup> littermate



**Figure 5. PU.1 directly binds cell cycle and protein synthesis genes repressed by IL-1.** (A) Experimental design for ChIP-seq experiment ( $n = 2/\text{group}$ ). (B) Heatmap showing PU.1 ChIP-seq peak intensities versus WCE control at TSS  $\pm 1$  kb. (C) Transcription factor binding site motif enrichment at ChIP-seq peak sites. (D) Pie chart comparing IL-1-downregulated genes identified in SLAM cells by RNA-seq analysis in Fig. 1 and presence of PU.1 peaks at or near these genes (TSS  $\pm 20$  kb). (E) Pie chart showing PU.1 peak locations in IL-1-downregulated genes. (F) Transcription factor binding site motif enrichment at PU.1 ChIP-seq peak sites in IL-1-downregulated genes (TSS  $\pm 20$  kb). (G) GO category enrichment of IL-1-downregulated DEGs containing PU.1 peaks in C. Representative genes from the indicated categories are shown to the right. Data are expressed as  $-\log_{10}$  P value. (H) UCSC genome browser rendering of a PU.1 peak location in *Myc* gene body. Tracks show PU.1 ChIP-Seq and WCE control, with corresponding peak locations and intensities in thioglycollate-elicited primary mouse macrophage (ThioMac) and BM-derived macrophage (BMDM) PU.1 ChIP-seq datasets from GSE21512. (I) *Myc* and PU.1 motif enrichment (motif score) at TSS  $\pm 1$  kb in IL-1-downregulated, -upregulated, or unchanged genes containing PU.1 peaks. Box shows upper and lower quartiles with line showing median value, and whiskers upper and lower 10th percentile and individual dots represent outliers. \*\*\*,  $P \leq 0.001$  based on Wilcoxon rank sum test. (J) Comparison of IL-1-downregulated genes in SLAM HSCs with genes containing PU.1 peaks within TSS  $\pm 20$  kb in PU-ER cells with or without 4-OHT. Based

on PU.1 ChIP-seq datasets in GSE21512. **(K)** GO category enrichment of IL-1-downregulated DEGs containing PU.1 peaks in PU-ER cell ChIP-seq dataset at 0 h +4-OHT versus combined 1–48 h +4-OHT. Top three GO categories are shown. Data are expressed as  $-\log_{10}$  P value. See also Fig. S4.

controls treated with or without IL-1 for 20 d by Fluidigm qRT-PCR array (Fig. 6 B). We confirmed a significant reduction of *Spi1* gene expression in *PU.1<sup>KI/KI</sup>* HSC<sup>LT</sup> (Fig. 6 D). *Cdk1*, *E2f1*, and *Myc* were overexpressed in *PU.1<sup>KI/KI</sup>* HSC<sup>LT</sup>, consistent with prior characterizations of *PU.1*-deficient HSCs under homeostatic conditions (Fig. 6, E and F; Rosenbauer et al., 2004; Staber et al., 2013). We observed increased expression of several cell cycle and protein synthesis genes, including *Ccne1*, *Ccna2*, and *Mki67* in *PU.1<sup>KI/KI</sup>* HSC<sup>LT</sup> (Fig. 6, E and F). Chronic IL-1 exposure further

increased expression of these genes in *PU.1<sup>KI/KI</sup>* HSC<sup>LT</sup> (Fig. 6, E and F). On the other hand, IL-1-mediated repression of other target genes, such as *Myc*, *Rpl9*, *Eif3a*, and *Fbl*, was attenuated or absent in *PU.1<sup>KI/KI</sup>* HSC<sup>LT</sup> (Fig. 6, E and F). We observed broadly similar patterns of aberrant gene expression in *PU.1<sup>KI/KI</sup>* HSC<sup>LT</sup> after acute IL-1 treatment in vivo (Fig. S5 A). These data suggest that PU.1 is required to limit the expression of cell cycle and protein synthesis genes both at steady state and under inflammatory stress.

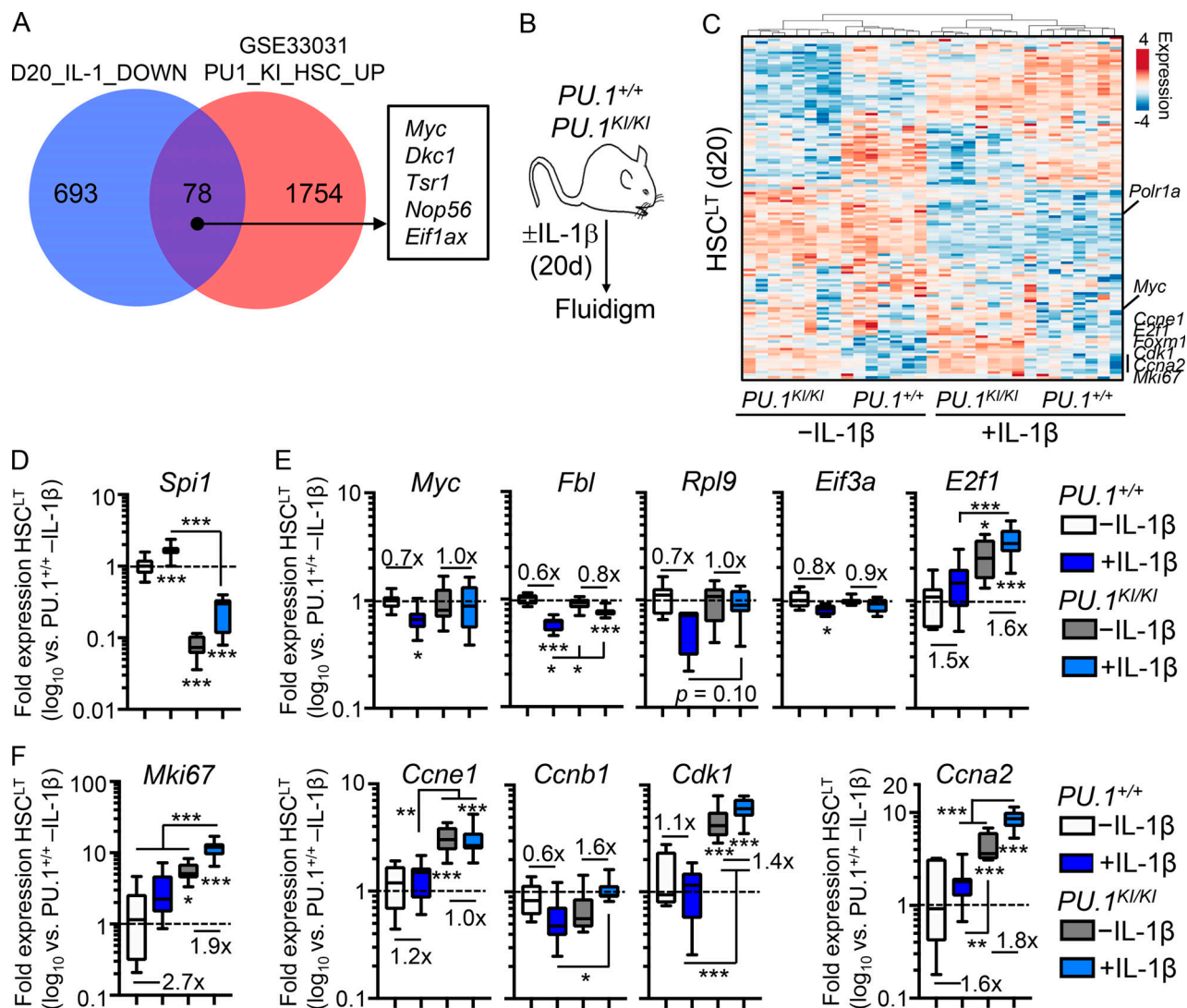


Figure 6. **Aberrant cell cycle and protein synthesis gene expression in *PU.1*-deficient HSC<sup>LT</sup>.** **(A)** Venn diagram comparing genes downregulated by IL-1 in SLAM cells (Fig. 1) and genes upregulated in *PU.1<sup>KI/KI</sup>* SLAM cells. **(B)** Experimental design of Fluidigm qRT-PCR array analyses of HSC<sup>LT</sup> from *PU.1<sup>+/+</sup>* and *PU.1<sup>KI/KI</sup>* mice treated with or without IL-1 $\beta$  for 20 d. **(C)** Heatmap with hierarchical clustering analysis (Pearson correlation with average linkage) of gene expression data from HSC<sup>LT</sup> in B. **(D)** Quantification by Fluidigm qRT-PCR array of *Spi1* gene expression in HSC<sup>LT</sup> from B. Data are expressed as  $\log_{10}$  fold expression versus -IL-1 $\beta$ . Box represents upper and lower quartiles with line representing median value. Whiskers represent minimum and maximum values. Data are representative of two independent experiments. **(E)** Quantification of cell cycle and protein synthesis gene expression by Fluidigm qRT-PCR array analysis in D. **(F)** Quantification of cell cycle gene expression by Fluidigm qRT-PCR array analysis in D. \*,  $P < 0.05$ ; \*\*,  $P < 0.01$ ; \*\*\*,  $P < 0.001$  by ANOVA with Tukey's test. See also Fig. S5.



### Chronic IL-1 induces aberrant cell cycle activity and expansion of $PU.1^{KI/KI}$ HSC<sup>LT</sup>

We next assessed how the molecular deregulations in  $PU.1^{KI/KI}$  HSC<sup>LT</sup> impacted the properties of these cells under inflammatory stress (Fig. 7 A). Consistent with our qRT-PCR data, IL-1-exposed  $PU.1^{KI/KI}$  HSC<sup>LT</sup> expressed higher relative levels of Myc than  $PU.1^{+/+}$  HSC<sup>LT</sup> (Fig. 7 B). Chronic IL-1 also triggered exuberant protein synthesis activity in  $PU.1^{KI/KI}$  HSC<sup>LT</sup> (Fig. 7 C). To assess the functional consequences, we assessed cell cycle activity in  $PU.1^{+/+}$  and  $PU.1^{KI/KI}$  HSC<sup>LT</sup>. Strikingly, IL-1 triggered increased cell cycle activity in  $PU.1^{KI/KI}$  HSC<sup>LT</sup> (Fig. 7 D). We independently confirmed IL-1-dependent activation of aberrant protein synthesis and cell cycle activity in HSC<sup>LT</sup> from conditional *SCL-Cre-ER::PU.1 $\Delta/\Delta$*  mice treated with or without IL-1 for 20 d (Fig. S5, B–D). In addition, consistent with our qRT-PCR analyses after acute IL-1 stimulation (Fig. S5 A), we found abnormally high cell cycle activity and Myc expression in  $PU.1^{KI/KI}$  HSC<sup>LT</sup> after single IL-1 injection (Fig. S5, E–G). Given that IL-1 triggered increased protein synthesis and cell cycle activity in  $PU.1$ -deficient HSC<sup>LT</sup>, we reasoned this could lead to aberrant expansion of the phenotypic HSC<sup>LT</sup> pool. We first addressed this question by monitoring HSC<sup>LT</sup> expansion using an expedient system in which  $PU.1^{KI/KI}$  HSC<sup>LT</sup> were cultured 1:1 with CD45.1<sup>+</sup> Boy/J HSC<sup>LT</sup>. Notably,  $PU.1^{KI/KI}$  HSC<sup>LT</sup> grew poorly in culture (Fig. S5 I); however, addition of IL-1 significantly potentiated the expansion of these cells (Fig. S5 I). In fact, immature c-Kit<sup>+</sup>/Sca-1<sup>+</sup> progenitors derived from  $PU.1^{KI/KI}$  HSC<sup>LT</sup> rapidly dominated the cultures relative to Boy/J competitor cells (Fig. S5, I and J). These data suggested that IL-1 might trigger expansion of  $PU.1^{KI/KI}$  HSC<sup>LT</sup> in vivo. Hence, we assessed the number of HSC<sup>LT</sup> in the BM of  $PU.1^{+/+}$  and  $PU.1^{KI/KI}$  mice treated with or without IL-1 for 20 d. As anticipated, IL-1 triggered aberrant expansion of phenotypic HSC<sup>LT</sup> exclusively in the BM of  $PU.1^{KI/KI}$  mice (Fig. 7 E). Notably, this phenotype was not confined to the BM, as we also observed significant expansion of phenotypic SLAM cells in the spleens of IL-1-treated  $PU.1^{KI/KI}$  mice (Fig. 7, F and G). Taken together, these data demonstrate that aberrant protein synthesis and cell cycle activity are emergent properties of  $PU.1$ -deficient HSC<sup>LT</sup> that can be triggered by IL-1 and result in the expansion of phenotypic HSC<sup>LT</sup> in the BM and extramedullary sites (Fig. 7 H). Altogether, these data show that  $PU.1$  is required to limit HSC<sup>LT</sup> cell cycle activity, thereby restricting HSC<sup>LT</sup> expansion during chronic inflammatory conditions.

## Discussion

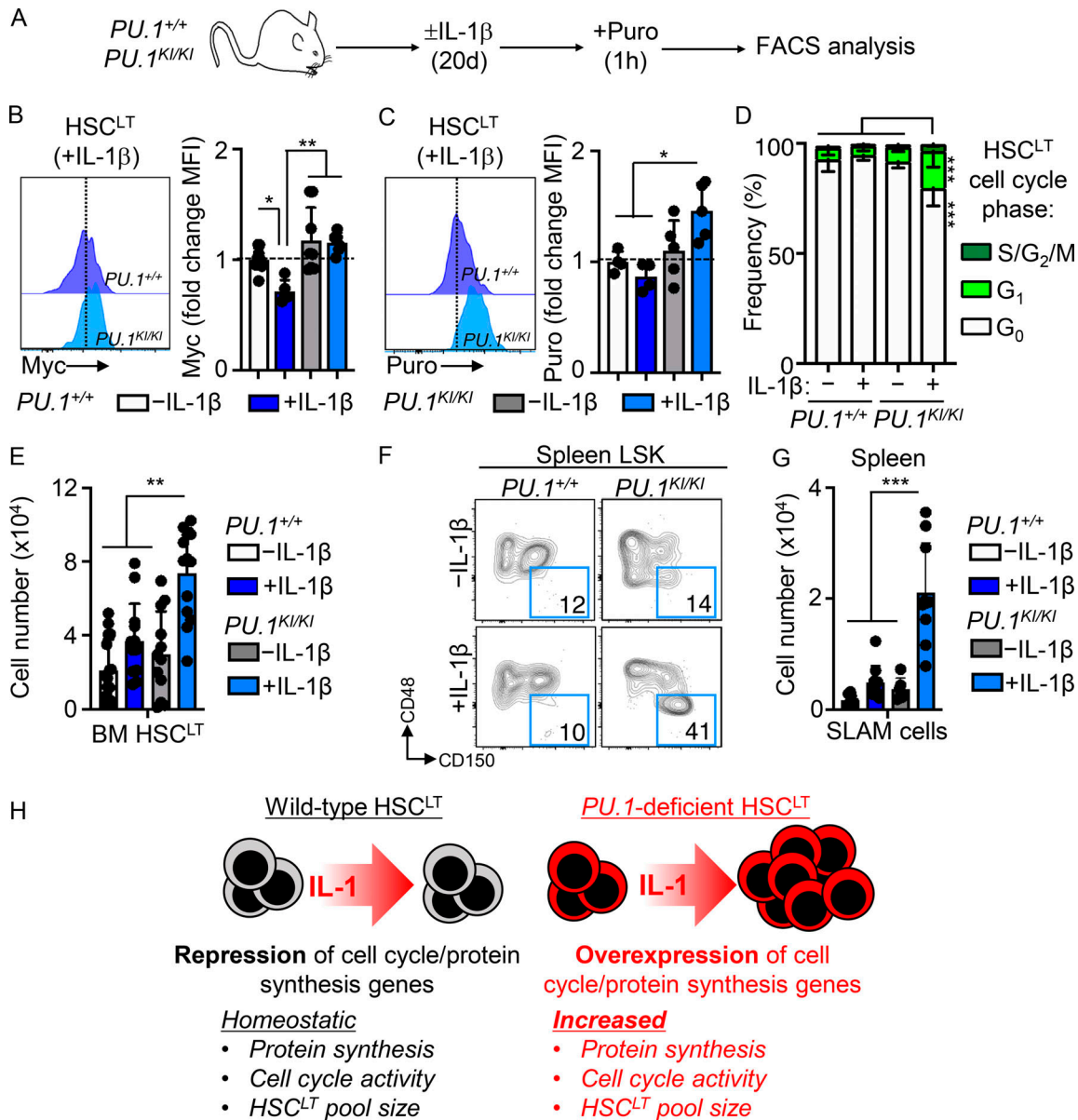
Here, we show that IL-1 exposure represses a broad set of genes regulating HSC<sup>LT</sup> cell cycle and protein synthesis activity. We show that this gene program is linked to restricted HSC<sup>LT</sup> cell cycle entry and thus underwrites the quiescent phenotype of HSCs under chronic inflammatory stress. Notably,  $PU.1$  is a crucial driver of this program, with  $PU.1$  itself binding the majority of target genes repressed by IL-1. Strikingly, our data demonstrate this molecular state leaves  $PU.1$ -deficient HSC<sup>LT</sup> poised to exit quiescence and support aberrant expansion of the phenotypic HSC<sup>LT</sup> pool when triggered by IL-1. Our data thus identify a  $PU.1$ -driven molecular mechanism enforcing HSC

quiescence during inflammatory stress and support a model in which  $PU.1$  serves as a critical limiting mechanism that regulates HSC cell cycle activity and pool size in this context.

We find that the IL-1/ $PU.1$  axis represses cell cycle and protein synthesis gene expression and limits HSC<sup>LT</sup> proliferative activity under all conditions studied, including in vitro culture and in vivo treatment of mice under both acute and chronic conditions. The activating versus suppressive functions of the IL-1/ $PU.1$  axis may at first appear paradoxical. Indeed, previous reports indicate that acute IL-1 administration in vivo triggers cell cycle activity in the SLAM compartment (Hemmati et al., 2019; Pietras et al., 2016; Weisser et al., 2016), which we recapitulate here. On the other hand, our H2B-GFP and cell cycle analyses show that only a limited fraction of phenotypic HSC<sup>LT</sup> enter the cell cycle following IL-1 challenge in vivo, particularly relative to the larger SLAM compartment, which is known to contain HSC-like CD41<sup>hi</sup> SLAM cells that can rapidly enter the cell cycle in response to acute inflammatory stress (Haas et al., 2015). Likewise, BrdU label-retention experiments show that, while stressors such as LPS can trigger proliferation in HSC-enriched cells, a sizeable fraction of these cells nonetheless retains the BrdU label (Takizawa et al., 2017; Wilson et al., 2008), and that a subset of CD49b<sup>lo</sup> HSCs that overlap phenotypically with the EPCR<sup>+</sup>/CD34<sup>-</sup> HSC<sup>LT</sup> fraction used here (Rabe et al., 2020) can remain dormant even following 5-fluorouracil myeloablation (Zhao et al., 2019). These data all support a model in which HSC<sup>LT</sup> engage mechanisms to limit cell cycling in response to inflammatory stress. Our findings that  $PU.1$ -deficient HSC<sup>LT</sup> cycle excessively following IL-1 stimulation indicate that  $PU.1$  is indeed one of these mechanisms. In this context, it is worth noting that published BM chimera studies show that in vivo HSC proliferation in response to IL-1 can be triggered independently of IL-1 receptor (IL-1R) on HSCs themselves (Cain et al., 2011; Ueda et al., 2009) and may rely on IL-1R-induced G-CSF production in the BM niche. Hence, the proliferative effect of IL-1 on HSC<sup>LT</sup> may in fact be the result of indirect mechanisms related to rapid mobilization of granulocytes from the BM, whereas direct IL-1 signaling triggers  $PU.1$ -dependent cell cycle restriction. Detailed studies using BM chimera models can further clarify the direct versus indirect effects of IL-1 on HSC<sup>LT</sup> proliferation in vivo.

We also previously reported that IL-1 activates precocious myeloid differentiation in HSCs (Pietras et al., 2016), and in the present study we see induction of myeloid genes in HSC<sup>LT</sup>; however, we demonstrate that IL-1 also activates a  $PU.1$  program that restricts HSC cell cycle activity and expansion by repressing a broad set of cell cycle and protein synthesis genes. We made similar observations in HSCs from mice with CIA (Hernandez et al., 2020). Repression of cell cycle and protein synthesis genes by  $PU.1$  may therefore be a common mechanism triggered in HSCs by at least a subset of inflammatory stimuli, including some TLRs, which share downstream signaling pathways with IL-1. On the other hand, analysis of HSCs from  $PU.1$ -EYFP mice treated acutely with TLR3 and -4 ligands polyriboinosinic: polyribocytidylic acid and LPS, respectively, show that  $PU.1$  is induced via a TNF-dependent mechanism (Etzrodt et al., 2019; Yamashita and Passegué, 2019). Furthermore, cytokines such as





**Figure 7. Chronic IL-1 induces aberrant cell cycle activity and expansion of PU.1-deficient HSC<sup>LT</sup>.** (A) Experimental design for analyses of HSC<sup>LT</sup> from PU.1<sup>+/+</sup> and PU.1<sup>KI/KI</sup> mice treated for 20 d with or without IL-1β. (B) Intracellular flow cytometry analysis of Myc protein levels in HSC<sup>LT</sup> from PU.1<sup>+/+</sup> and PU.1<sup>KI/KI</sup> mice treated with or without IL-1β for 20 d (n = 4–9/group). Data are expressed as fold change of MFI versus –IL-1β. Individual values are shown with bars representing mean values. Data are compiled from two independent experiments. (C) Intracellular flow cytometry analysis of puro incorporation in HSC<sup>LT</sup> from PU.1<sup>+/+</sup> and PU.1<sup>KI/KI</sup> mice treated with or without IL-1β for 20 d (n = 4 PU.1<sup>+/+</sup>; 5 PU.1<sup>KI/KI</sup>). Data are expressed as fold change of MFI versus –IL-1β. Individual values are shown with bars representing mean values. Data are from one experiment. (D) Quantification of cell cycle phase distribution in HSC<sup>LT</sup> from mice in A. Data are compiled from two independent experiments. (E) Quantification of BM HSC<sup>LT</sup> from mice in A. Individual values are shown with bars representing mean values. Data are compiled from three independent experiments. (F) Representative FACS plots showing SLAM cells in the spleens of PU.1<sup>+/+</sup> and PU.1<sup>KI/KI</sup> mice treated for 20 d with or without IL-1β. (G) Quantification of SLAM cells in the spleens of mice in A. Individual values are shown with bars representing mean values. Data are compiled from two independent experiments. (H) Cartoon showing key features of WT and PU.1-deficient HSC<sup>LT</sup>. WT HSC<sup>LT</sup> (left) engage a cell cycle and protein synthesis repression gene program that limits protein synthesis, cell cycle activity, and HSC<sup>LT</sup> pool size following challenge with IL-1. On the other hand, PU.1-deficient HSC<sup>LT</sup> overexpress cell cycle and protein synthesis genes, priming them for increased protein synthesis and cell cycle activity that is associated with aberrant expansion of the HSC<sup>LT</sup> pool following IL-1 challenge. \*, P < 0.05; \*\*, P < 0.01; \*\*\*, P < 0.001 by ANOVA with Tukey's test. Error bars represent SD. See also Fig. S5.

IFN do not robustly activate PU.1 expression in a direct fashion (Etzrodt et al., 2019), suggesting that other mechanism(s) may enforce HSC quiescence under chronic IFN stimulation, such as activation of p53 and/or the mRNA translation-blocking activity of several IFN-stimulated genes (Li et al., 2015; Pietras et al., 2014).

It is important to note that, while PU.1 is commonly characterized as a lineage differentiation factor, its role as a regulator of cell proliferation has also been extensively studied (Delestré et al., 2017; Fukuchi et al., 2008; Oikawa et al., 1999; Solomon et al., 2017; Ziliotto et al., 2014). The connection between cell

cycle inhibition and myeloid differentiation likely centers on cell cycle lengthening as a mechanism to promote PU.1 accumulation and myeloid differentiation in hematopoietic progenitors (Kueh et al., 2013). In agreement with this model, our data show that increased PU.1 activity serves as more of a rheostat than a bona fide proliferation block in HSC<sup>LT</sup>, erecting enough of an activation barrier to prevent excessive proliferation during inflammatory challenge while still priming HSCs for myeloid differentiation as evidenced by simultaneous upregulation of myeloid determinant genes in IL-1-exposed HSC<sup>LT</sup>. This is a function common to numerous myeloid transcription factors, including *Cebpa* family members and *Gfi1*, which is itself a PU.1 target (Hock et al., 2004; Porse et al., 2005; Pulikkan et al., 2017; Staber et al., 2013; Umek et al., 1991; Zeng et al., 2004). Thus, induction of a PU.1-dependent cell cycle restriction gene program in HSC<sup>LT</sup> under inflammatory stress conditions is consistent with a model in which PU.1 promotes efficient generation of myeloid progenitors to reconstitute hematopoiesis, while protecting the HSC compartment from damage and/or depletion. Absence of this program likely underlies the failure of *PU.1<sup>KI/KI</sup>* mice to reconstitute hematopoiesis following 5-fluorouracil treatment (Staber et al., 2013), which we interpret as a coupled effect of increased HSC proliferation leading to apoptosis, and inefficient generation of new myeloid progenitors due to reduced PU.1 accumulation. Altogether, this mechanism may be a remarkable example of parsimony in a biological system, wherein a single molecular program can mediate distinct functional outcomes based on cell type and context.

Our data agree with prior studies showing that PU.1 deficiency leads to derepression of *Myc* and numerous cell cycle genes, including *Cdk1* and *E2f1* (Rosenbauer et al., 2004; Staber et al., 2013; Will et al., 2015), which is exacerbated by IL-1 exposure. Indeed, we find that PU.1 directly binds a wide array of genes that regulate cell cycle and protein synthesis activity. In that setting, it is unlikely that repression of a single factor, such as *Myc*, is the sole mechanism limiting HSC<sup>LT</sup> cell cycle activity. Indeed, we find that inhibition of protein synthesis in cultured HSC<sup>LT</sup> using *Oma* phenocopies the delayed cell cycle entry observed with IL-1 stimulation, which is consistent with our model that PU.1 inhibition of multiple protein synthesis genes contributes to enforced HSC quiescence. Notably, *Oma* is a U.S. Food and Drug Administration-approved therapy for chronic myelogenous leukemia and can directly ablate MDS stem cells with aberrant levels of protein synthesis (Stevens et al., 2018). Protein synthesis and cell cycle activity are closely linked, as cell cycle entry and mitosis require a significant amount of new protein. Hence, in eukaryotic cells, deletion and/or knockdown of key genes regulating protein synthesis, such as translation elongation initiation factors (eIFs), several of which are repressed by IL-1 in our dataset, results in delayed cell cycle entry (Polymenis and Aramayo, 2015). The importance of eIFs in initiating HSC cell cycle activity has been illustrated by elegant work in which dual deletion of *4E-BP1/2*, which negatively regulates translation by inhibiting eIF4E, leads to increased protein synthesis, aberrant cell cycle activity, and HSC expansion (Signer et al., 2016). Likewise, deletion of *Pten*, which dephosphorylates and inhibits the eIF activator mammalian target of

rapamycin, leads to similar aberrant HSC activity and hypersensitivity to inflammatory factors, such as G-CSF and IFN (Porter et al., 2016; Signer et al., 2014), indicating that protein synthesis levels must be carefully regulated for normal HSC function. The phenotype of *Pten*- and *4E-BP1/2*-deficient HSCs is strikingly reminiscent of that of IL-1-exposed PU.1-deficient HSC<sup>LT</sup> in our model. In a similar line, inflammatory initiation of a cell cycle-primed *G<sub>al</sub>ert* state in HSCs and other cells requires activation of mammalian target of rapamycin (Rodgers et al., 2014). We also identified decreased expression of ribosomal RNA genes, as well as genes such as *Fbl* required to process them for assembly into ribosomes. While cells synthesize ribosomes independently of cell cycle phase, inhibition of rRNA production can halt cell cycle activity (Polymenis and Aramayo, 2015) with accompanying decreases in cell size, similar to our findings in HSC<sup>LT</sup> exposed to IL-1 and/or *Oma* in culture. Along these lines, HSCs carrying a hypomorphic allele of the ribosomal protein *Rpl24* exhibit decreased proliferative activity and can rescue the phenotype of *Pten*-deficient HSCs (Signer et al., 2014). Likewise, IL-1 downregulates expression of *Myc*, a crucial upstream regulator of protein synthesis and cell cycle genes that leads to defective cell cycle entry if deleted in stem cells (Laurenti et al., 2008; Scognamiglio et al., 2016; Wilson et al., 2004). Together, these data suggest that fine tuning of protein synthesis is essential for maintaining HSC quiescence and function (Signer et al., 2014). Interestingly, despite IL-1-mediated downregulation of protein synthesis genes and slowed cell cycle progression in our in vitro cultures, we do not observe decreased protein synthesis rates in IL-1-exposed HSC<sup>LT</sup> in vivo. Repression of protein synthesis genes may therefore dampen the effects of IL-1-driven mitogenic signaling and maintain homeostatic protein synthesis activity rather than block it altogether, which in vitro is read out as slowed cell cycle progression in response to the stress of being placed in culture. IL-1 activates numerous signaling pathways that directly impact protein synthesis and cell cycle activity, including PI3K/Akt, p38 MAPK, MAPK/ERK kinase (MEK)/ERK, and RAS (Dinarelli, 2018). Thus, in future studies, we hope to identify which pathway(s) are potential triggers that activate aberrant protein synthesis and cell cycle activity in *PU.1*-deficient HSCs, as well as the extent to which inhibiting them can rescue this phenotype.

Dysregulated inflammatory signaling has emerged as a key partner alongside oncogenic mutations in the development and/or progression of hematological malignancy (Barreyro et al., 2018; Pietras, 2017). Aberrant signaling via IL-1 and the downstream IL-1 receptor associated kinase/TNF receptor associated factor pathway shared by IL-1R and TLRs has been implicated as a driver of survival and/or expansion of MDS and myeloid leukemia stem cells (Ågerstam et al., 2016; Askmyr et al., 2013; Barreyro et al., 2012; Carey et al., 2017; Muto et al., 2020; Smith et al., 2019; Zhang et al., 2016). Indeed, blockade of these pathways can limit and/or reverse disease progression (Carey et al., 2017; Mitchell et al., 2018; Rhyasen et al., 2013; Zhang et al., 2016); however, the mechanism(s) by which inflammatory signaling initiates expansion of oncogenically mutated HSCs remain obscure. Chronic inflammation, often associated with increased IL-1 activity, is a common phenotype in individuals at

risk for hematological malignancy, which can be related to several preexisting factors, including aging/tissue decline, genotoxin exposure, metabolic dysfunction, and/or autoimmune disease (Barreyro et al., 2018; Pietras, 2017). Our data suggest that, while chronic IL-1 exposure can induce expansion of myeloid-biased hematopoietic progenitors and mature myeloid cells, this phenotype is essentially self-limiting and does not deterministically progress to malignancy. These data are consistent with the overall rarity of hematological malignancy among individuals with chronic inflammatory phenotypes, despite the relative increase in risk (Anderson et al., 2009; Gañán-Gómez et al., 2015). On the other hand, loss-of function mutations in *PU.1* itself are rarely observed in hematological malignancy, although a wide array of myeloid leukemia-associated oncogenic lesions can interfere with PU.1 expression or function, including *PML/RARA*, *AML1-ETO*, *NPM1c*, *CEBPA*, and mitogenic kinase mutations in *BCR/ABL* and *Flt3<sup>ITD</sup>* (Gerloff et al., 2015; McKenzie et al., 2019; Mueller et al., 2006; Noguera et al., 2016; Vangala et al., 2003; Yang et al., 2012). In addition, *TET2* and/or *DNMT3A* mutations associated with early oncogenesis may interfere with PU.1 function due to aberrant methylation of PU.1 binding sites (Kaasinen et al., 2019). Hence, deficiency in key myeloid regulators, like PU.1, related to indirect effects of mutations in other genes may serve as a crucial nexus that primes HSCs to activate aberrant protein synthesis and cell cycle activity when triggered by inflammatory signals associated with BM pathogenesis, like IL-1 and TNF- $\alpha$ . This model is illustrated by a parallel study by our group in which we found that IL-1 can trigger the selective expansion of *Cebpa*-deficient HSPCs in a mouse model of oncogenic BM competition (Higa et al., 2021). These findings are consistent with the theory of adaptive oncogenesis, which stipulates that environmental factors associated with tissue decline, such as inflammation, are crucial drivers of oncogenesis by selecting for emergent phenotypes, such as increased proliferation, self-renewal, or survival, that are linked cancer-associated mutations (Henry et al., 2015; Laconi et al., 2020). Hence, oncogenic mutations and inflammatory signals may collaborate to activate emergent proliferative phenotypes in stem cells that, in turn, lead to aberrant expansion of downstream progenitors and myeloid cells that can initiate disease. Such a model provides a rationale for exploring the use of anti-inflammatory therapies as a means of preventing and/or delaying leukemogenesis in at-risk individuals.

## Materials and methods

### Mice

WT C57BL/6, congenic B6.SJL-*Ptprca<sup>a</sup>Pepc<sup>b</sup>*/BoyJ (Boy/J) mice, *GFP-Myc* mice (Huang et al., 2008), and *Col1a1-TetO::rtTA-H2B-GFP* mice (Foudi et al., 2009) were obtained from The Jackson Laboratory. *PU.1<sup>KI/KI</sup>* mice and *PU.1<sup>fllox</sup>* mice (Staber et al., 2013) were a kind gift of Dan Tenen (Harvard Stem Cell Institute, Cambridge, MA). *PU.1<sup>fllox</sup>* mice were crossed onto a 4-OHT-inducible *SCL-Cre<sup>ERT</sup>* driver strain (Göthert et al., 2005) for experiments. *PU.1-EYFP* mice (Hoppe et al., 2016; Kirstetter et al., 2006) were a kind gift of Dr. Claus Nerlov (MRC Weatherall Institute, Oxford, UK). *PU.1ERT2* mice (Fukuchi et al., 2008) were kindly provided by

Dr. Hideyaki Nakajima (Department of Stem Cell and Immune Regulation, Yokohama City University School of Medicine, Yokohama, Japan). WT littermate controls were used for experiments involving *PU.1<sup>KI/KI</sup>* mice and *PU.1<sup>fllox</sup>* mice. 6–12-wk-old animals of both sexes were used for experiments. All animal experiments were conducted in accordance with a protocol approved by the Institutional Animal Care and Use Committee at University of Colorado Anschutz Medical Campus (protocol no. 00091).

### In vivo procedures

For in vivo IL-1 stimulation, IL-1 $\beta$  (Peprotech) was resuspended in sterile Dulbecco's PBS/0.2% BSA. 0.5  $\mu$ g IL-1 or PBS/BSA alone was injected i.p. in a 100- $\mu$ l bolus once per day for either 1 or 20 d, as previously described (Pietras et al., 2016; Rabe et al., 2020). In vivo puro labeling assays were performed as previously described (Chapple et al., 2018), with 500  $\mu$ g puro (Life Technologies) injected i.p. 1 h before euthanasia. In vivo H2B-GFP labeling was performed by feeding mice with doxycycline chow (2 g/kg; Teklad) ad libitum for 2 wk (Säwén et al., 2016). Animals were allowed to rest for 1 wk before IL-1 treatment. Induction of the *SCL-Cre<sup>ERT</sup>* transgene in PU.1 conditional KO mice was performed by injecting mice i.p. with 25 mg/kg 4-OHT resuspended in corn oil daily for 3 d. Mice were allowed to rest for 1 wk before the start of IL-1 treatment.

### Flow cytometry

Analysis of BM cell populations was performed using a similar protocol as previously described (Pietras et al., 2016; Rabe et al., 2020). BM was flushed from femurs and tibiae of mice using staining media (SM; Hanks' Buffered Saline Solution + 2% FBS) and a syringe equipped with a 21-G needle. Cells were subsequently resuspended in 1 $\times$  ACK (150 mM NH<sub>4</sub>Cl/10 mM KHCO<sub>3</sub>) to remove erythrocytes, washed with SM, filtered through 70- $\mu$ m mesh to remove debris, resuspended in SM, and counted on a Vicell automated counter (Beckman Coulter). For quantification of immature HSPCs, 10<sup>7</sup> BM cells were blocked with purified rat IgG (Sigma-Aldrich) and stained for 30 min on ice with SM containing the following antibodies: PE-Cy5-conjugated anti-CD3, CD4, CD5, CD8, Gr-1, and Ter119 as a lineage exclusion stain; Flk2-biotin; CD34-FITC; EPCR (endothelial protein C receptor)-PE; Mac-1-PE/Cy7; CD16/32-APC; CD48-A700; and cKit-APC/Cy7. Cells were subsequently washed, resuspended in a 1:4 dilution of Brilliant Staining Buffer (Becton Dickinson) in SM containing Sca-1-BV421, CD41-BV510, CD105-BV711, CD150-BV785, and streptavidin (SA)-BV605 and incubated for 30 min on ice. For analysis of *GFP-Myc::PU.1-EYFP* cells, a custom 510/20-nm (GFP) and 550/30-nm (EYFP) bandpass filter setup (Becton Dickinson) was used to discriminate the two fluorescent proteins. BM cells from single-positive mice were used for compensation controls and fluorescence-minus-one controls, and GFP<sup>-</sup>/YFP<sup>-</sup> BM cells were surface stained alongside and used as negative controls. For analysis of mature BM cell populations, cells were blocked as above and stained for 30 min on ice with the following antibodies: Gr-1-Pacific Blue, Ly6C-BV605, B220-BV786, CD4-FITC, CD8-PE, Mac-1-PE/Cy7, IgM-APC, CD3-A700, and CD19-APC/Cy7. Following surface staining, cells were



washed with SM, resuspended in SM containing 1  $\mu\text{g}/\text{ml}$  propidium iodide, and immediately analyzed on a three-laser, 12-channel FACSCelesta analyzer (Becton Dickinson) or a five-laser, 18-channel BD Fortessa. For analysis of spleen cells, spleens were removed and minced through a 70- $\mu\text{m}$  filter basket (VWR) to make a single-cell suspension. Splenocytes were treated with ACK buffer as above and subsequently processed for staining of mature and immature hematopoietic populations, as described above.

Cell cycle analysis was performed using protocols similar to previous publications (Hernandez et al., 2020; Jalbert and Pietras, 2018).  $10^7$  BM cells were stained for 30 min on ice with the following antibodies: PE-Cy5-conjugated anti-CD3, CD4, CD5, CD8, Gr-1 and Ter119 as a lineage exclusion stain, Flk2-biotin, CD34-FITC, EPCR-PE, Sca-1-PE/Cy7, CD48-A700, and c-Kit-APC/Cy7. Cells were washed with SM and resuspended in 1:4 Brilliant Buffer:SM containing SA-BV605 and CD150-BV785, incubated for 30 min on ice, washed in SM, and fixed for 20 min at room temperature (RT) with Cytofix/Cytoperm (Becton Dickinson). Cells were subsequently washed with 1 $\times$  PermWash buffer (Becton Dickinson), permeabilized for 10 min at RT with Perm Buffer Plus (Becton Dickinson), washed in PermWash, and refixed for 5 min at RT with CytoFix/Cytoperm. Cells were subsequently washed in PermWash and incubated with anti-Ki-67 antibody in PermWash buffer for 30 min at RT. Cells were then washed and either stored at 4°C or resuspended in Dulbecco's PBS containing 1  $\mu\text{g}/\text{ml}$  DAPI and analyzed on a BD LSRII analyzer equipped with a UV laser (Becton Dickinson).

Myc staining was performed as previously described (Freire and Conneely, 2018).  $10^7$  BM cells were stained for 30 min on ice with SM containing the following antibodies: PE-Cy5-conjugated anti-CD3, CD4, CD5, CD8, Gr-1 and Ter119 as a lineage exclusion stain, Flk2-biotin, CD34-FITC, EPCR-PE, Mac-1-PE/Cy7, CD48-A700, and cKit-APC/Cy7. Cells were washed in SM and then stained for 30 min in 1:4 Brilliant Buffer:SM containing Sca-1-BV421, SA-BV605, and CD150-BV785. Cells were subsequently washed in SM and fixed for 20 min with CytoFix/CytoPerm. Cells were washed with PermWash and blocked in PermWash for 1 h at RT, followed by washing and a 1-h RT incubation with anti-Myc purified antibody. Cells were subsequently stained with an A647-conjugated anti-rabbit Fab for 30 min at RT, washed in PermWash, resuspended in SM, and analyzed on an LSRII.

Puro stainings were performed as previously described (Chapple et al., 2018). Cells were surface stained and fixed using the same approach as for Myc staining. Following fixation, cells were stained with anti-puro antibody diluted in PermWash buffer for 1 h at RT, washed and stained with an anti-mouse IgG2a antibody for 30 min, washed once more, and resuspended in SM for analysis on an LSRII.

For H2B-GFP dilution analysis, we used splenocytes from Ubc-GFP mice (Schaefer et al., 2001) as a GFP compensation control to ensure comparable brightness to the GFP signal. BM cells were stained as above and analyzed on an LSRII or sorted on a FACS Aria Fusion sorter. GFP dilution analyses were performed by using the proliferation analysis function of FlowJo using default settings. All samples from an individual

experiment were concatenated before running the algorithm, and GFP expression bins were subsequently assigned to individual samples.

All fluorescence intensity data throughout the manuscript are based on the geometric mean fluorescence intensity (MFI) of that parameter. A complete list of FACS antibodies and dilutions used can be found in Table S6.

### Cell sorting

For HSC isolation by cell sorting, arm, leg, pelvic bones, and spines were isolated from mice as previously described (Pietras et al., 2016; Rabe et al., 2020). Bones were crushed in SM using a mortar and pestle and depleted of erythrocytes with 1 $\times$  ACK. Cells were subsequently placed atop a Histopaque 1119 gradient (Sigma-Aldrich) and centrifuged. To enrich c-Kit<sup>+</sup> cells, BM cells were incubated on ice for 20 min with c-Kit microbeads (5  $\mu\text{l}$ /100  $\mu\text{l}$  SM per mouse; 130-091-224; Miltenyi Biotec), washed with SM, and enriched on an AutoMACS Promagnetic cell separator (Miltenyi Biotec). Enriched cells were subsequently washed, blocked with rat IgG, and stained for 30 min on ice with the following antibodies: PE-Cy5-conjugated anti-CD3, CD4, CD5, CD8, Gr-1, and Ter119 as a lineage exclusion stain, Flk2-biotin, CD34-FITC, EPCR-PE, Mac-1-PE/Cy7, CD48-A700, and c-Kit-APC/Cy7. Cells were subsequently washed with SM and resuspended in a 1:4 dilution of Brilliant Staining Buffer in SM containing Sca-1-BV421, SA-BV605, and CD150-BV785. For B220<sup>+</sup> cell isolation by cell sorting, spleens were harvested, pressed over a 70- $\mu\text{m}$  filter, and depleted of erythrocytes. To enrich for B220<sup>+</sup> cells, splenocytes were incubated on ice for 20 min with B220 microbeads (20  $\mu\text{l}$ /1,000  $\mu\text{l}$  SM per mouse; Miltenyi Biotec), washed with SM, and enriched on an AutoMACS Pro. Enriched cells were washed, blocked with rat IgG, and stained with B220-APC for 15 min on ice. Purified B220<sup>+</sup> cells were immediately fixed for 20 min at RT (100  $\mu\text{l}$ ; BD Cytofix/Cytoperm), washed with SM, and stored at 4°C.

### In vitro culture assays

Purified HSC<sup>LT</sup> were cultured using a similar protocol as that previously published (Pietras et al., 2016). Double-sorted cells were grown in StemPro34 containing Stempro supplement, antibacterial-antimycotic (100 $\times$ ; Gibco), L-glutamine (100 $\times$ ; Gibco), stem cell factor (SCF; 25 ng/ml), thrombopoietin (TPO; 25 ng/ml), IL-3 (10 ng/ml), GM-CSF (20 ng/ml), Flt3L (50 ng/ml), IL-11 (50 ng/ml), erythropoietin (4 U/ml), and IL-1 $\beta$  (25 ng/ml) and were incubated at 37°C, 5% O<sub>2</sub>, 5% CO<sub>2</sub> for either 12 or 24 h. Cell culture grade puro (1 nM; Gibco) was added 1 h before harvesting cells to monitor protein synthesis rates. In experiments containing Oma (100 nM; Teva Pharmaceuticals), cells were cultured in the presence of Oma for 1 h before IL-1 $\beta$  addition and remained in cultures for the duration of the experiment. Following indicated times in culture, cells were harvested and either resorted based on viability for Fluidigm gene expression analysis or were immediately fixed for 20 min at RT (100  $\mu\text{l}$ ; BD Cytofix/Cytoperm) for Ki-67/DAPI analysis or puro incorporation assays. Following fix/perm, 5  $\times$  10<sup>5</sup> sorted, fixed B220<sup>+</sup> spleen cells were added to each sample as carrier cells and excluded during analysis based on B220 expression (Matatall et al.,



2018). *PU.1-ERT HSC<sup>LT</sup>* were cultured as above but with or without 100 nM 4-OHT. PU-ER cells were cultured in Iscove's Modification of Dulbecco's medium (IMDM) + 10% heat-inactivated serum and 5 mg/ml IL-3 and GM-CSF. Transgene was induced by resuspending cells in media containing 100 nM 4-OHT. Cells were harvested after 24 h and analyzed for cell cycle activity or Myc expression levels as described above.

#### Luciferase reporter assays

*pcDNA3-PU.1* (human PU.1) and *pXP2-MYC* luciferase reporter constructs were kind gifts of Dan Tenen (Harvard Stem Cell Institute). *pXP2-MYC* contains the 2.5-kb *Xmn1* fragment of the human *MYC* promoter driving a luciferase reporter. 293T cells were transfected with *pXP2-Myc* and either *pcDNA3-PU.1* or empty *pcDNA3* using PolyJet in vitro DNA transfection reagent (Signagen) according to the manufacturer's instructions. 24 h later, cells were lysed and analyzed for luciferase activity using the Pierce Firefly Luciferase Glow Assay (Invitrogen). Luciferase activity was read out on a microplate reader (Promega).

#### Single-cell tracking analysis

Time-lapse experiments were conducted at 37°C, 5% O<sub>2</sub>, 5% CO<sub>2</sub> on  $\mu$ -slide VI<sup>0.4</sup> channels slides (IBIDI) coated for 1 h at RT with 5 or 10  $\mu$ g/ml anti-CD43-biotin, as previously described (Loeffler et al., 2018). Cells were cultured in phenol red-free IMDM supplemented with 20% bovine serum albumin/human insulin/human transferrin, 2 mM L-glutamine, 50  $\mu$ M 2-mercaptoethanol and 50 U/ml penicillin, 50  $\mu$ g/ml streptomycin, 25 ng/ml SCF, 25 ng/ml TPO, 10 ng/ml IL-3, 20 ng/ml GM-CSF, 50 ng/ml Flt3L, 50 ng/ml IL-11, and 4 U/ml EPO. 25 ng/ml IL-1b and/or 500 nM 4-OHT (Sigma-Aldrich) was added as indicated. Images were acquired using a Nikon-Ti Eclipse equipped with a linear encoded motorized stage, Orca Flash 4.0 V2 (Hamamatsu), Spectra X fluorescent light source (Lumencor), and The Cube (Life Imaging Service) temperature control system. White light emitted by Spectra X was collimated and used as a transmitted light for brightfield illumination via a custom-made motorized mirror controlled by Arduino UNO Rev3 (Arduino). Fluorescent images were acquired using optimized filter sets eGFP (470/40 nm; 495LP; 525/50 nm), YFP (500/20 nm; 515LP; 535/30 nm), mKO2 (546/10 nm; 560LP; 577/25 nm), mCherry (550/32 nm; 585LP; 605/15 nm), and Cy5 (620/60 nm; 660LP; 700/75 nm; all AHF) to detect GFP-cMYC, PU.1-YFP, CD71-PE, tetramethylrhodamine, and CD71-APC, respectively. Time intervals of brightfield and fluorescent image acquisition were chosen to minimize phototoxicity. Images were acquired using a 10 $\times$  CFI Plan Achromat  $\lambda$  objective (NA 0.45). Single-cell tracking and image quantification were performed using self-written software as described (Hilsenbeck et al., 2016; Loeffler et al., 2018). Software used for data acquisition of time-lapse imaging data is published and open sourced (YouScope v.2.1; <http://langmo.github.io/youscope/>). Software for single-cell tracking and fluorescence quantification used in this study is published and open sourced (Hilsenbeck et al., 2016). Segmentation software is published and open sourced (Hilsenbeck et al., 2017). Acquired 16-bit images with 2048  $\times$  2048-pixel resolution were saved as .png and linearly transformed to 8-bit using

channel-optimized white points and corrected for background and shading (Peng et al., 2017) before analysis. Brightfield images were used for segmentation using fastER (Hilsenbeck et al., 2016), eroded to reduce segmentation artifacts caused by close cell proximity (settings: morphological transformation  $x = 3$ ,  $y = 3$ ,  $op = 2$ , shape: 2), and subsequently dilated (settings: simple dilation 6) to ensure proper segmentation and quantification results. Tracking and quantification of fluorescence channels were done as previously described (Hilsenbeck et al., 2016) and analyzed using Matlab 2018b (MathWorks). For hierarchical clustering analyses, PU.1YFP expression levels of in vitro-cultured HSCs were quantified from the start of culture until cell division. PU.1YFP fluorescence intensities were z-normalized across replicates, with each single-cell time series normalized to 40 time points using Matlab's spline function and clustered using hierarchical clustering with Euclidean distance and ward linkage using Matlab 2019b. The number of clusters was chosen based on (1) the reproducibility of cluster frequencies across replicates and (2) to minimize intracluster variance.

#### RNA-seq

RNA was isolated from individual pools of 10<sup>4</sup> to 2  $\times$  10<sup>4</sup> double-sorted SLAM cells using an RNEasy Micro kit (Qiagen). RNA was quantified and quality checked using an Agilent Bioanalyzer 2100 (Agilent Technologies). 1 ng of total RNA was preamplified using the SMARTer Ultra-Low Input kit v4 (Clontech) according to the manufacturer's instructions, and cDNA quality was assessed using the Qubit Fluorometer (Life Technologies) and the Bioanalyzer. 150 pg cDNA was used to generate Illumina sequencing libraries using the NexteraXT kit (Illumina) according to the manufacturer's instructions. Libraries were subsequently hybridized to an Illumina single-end flow cell and amplified using cBot (Illumina). Sequencing of libraries was performed on Illumina HiSeq 2500v4 high-throughput sequencer. Single-ended reads of 100 nt were generated for each sample and demultiplexed using bcl2fastq v1.8.4. Trimmomatic v0.32 was used for quality filtering and adapter removal. Processed reads were mapped to the mouse genome GRCm38.p4 (mm10/mg38) using STAR 2.4.2a. Raw read counts were obtained via htseq-count v0.6.1 and Gencode-M12 gene annotations. Differential expression analyses were performed using deSeq2 in Bioconductor. Genes with  $P_{adj} < 0.05$  were considered significant DEGs. Upstream regulator analysis of DEGs was performed using IPA software on default settings. GSEA analyses were performed on DEGs using default settings. GO analyses were performed using DAVID v6.8 (<http://david.ncifcrf.gov/>; Huang et al., 2009). Venn diagrams were generated from DEG lists using InteractiVenn ([http://www.interactivenn.net](http://www.interactivenn.net;); Heberle et al., 2015).

#### ChIP-seq

ChIP-seq analysis was performed on LSK/Flk2-/CD150<sup>+</sup> cells sorted from the BM of eight C57BL/six mice per ChIP. Cells were cross-linked in 0.75% formaldehyde, pelleted, and frozen until the ChIP procedure. Pellets were thawed on ice, resuspended in lysis buffer (1% SDS, 10 mM EDTA, 50 mM Tris-HCl [pH 8.1] plus protease inhibitor) for 10 min. Volume was brought up to 1 ml with ChIP dilution buffer (16.7 mM Tris-HCl [pH 8.1],

167 mM NaCl, 0.01% SDS, 1.1% Triton X-100, and 1.2 mM EDTA plus protease inhibitor) and samples were sonicated with a Branson sonicator to shear chromatin. Chromatin was subsequently incubated with 1  $\mu$ g PU.1 antibody (sc-390405; Santa Cruz Biotechnology) and rotated overnight at 4°C. Next, ChIPs were added to a 50:50 mix of prewashed Protein A/G Dynabeads (50  $\mu$ l; 10001D/10009D; Thermo Fisher Scientific) and rotated overnight at 4°C. The next day, 175  $\mu$ l RIPA/140 mM NaCl buffer (0.1% sodium deoxycholate, 0.1% SDS, 1% Triton X-100, 140 mM NaCl, 1 mM EDTA, 20 mM Tris-HCl [pH 8.1]) was added to each tube and beads were transferred to a 96-well plate on a magnet, washed twice with cold RIPA/500 ml NaCl buffer (0.1% sodium deoxycholate, 0.1% SDS, 1% Triton X-100, 140 mM NaCl, 1 mM EDTA, and 20 mM Tris-HCl [pH 8.1]), twice with cold LiCl buffer (0.25 M LiCl, 1% NP-40, 1% Na deoxycholate, 1 mM EDTA, and 10 mM Tris-HCl [pH 8.1]), and twice with RT TE buffer (10 mM Tris-HCl [pH 8.0] and 1 mM EDTA [pH 8.0]). Chromatin was eluted by adding 50  $\mu$ l of elution buffer (10 mM Tris-Cl [pH 8.0], 5 mM EDTA, 300 mM NaCl, 0.1% SDS, and 5 mM dithiothreitol) and 8  $\mu$ l of reverse cross-linking buffer (250 mM Tris-HCl [pH 6.5], 1.25 M NaCl, 62.5 mM EDTA, 5 mg/ml Proteinase K, and 62.5  $\mu$ g/ml RNase A) and incubated at 65°C overnight. ChIP material was quantified on a Qubit spectrometer (Invitrogen) according to manufacturer's instructions. Library construction was performed first using an End-it DNA End-Repair Kit (ER0720; Epicenter) according to manufacturer's instructions, followed by DNA ligase-based adapter ligation (M2200S; New England Biolabs) and enrichment of adapter-modified DNA fragments by PCR. PCR fragments were gel purified using a Qiagen Gel Purification Kit (Qiagen) and sequenced on an Illumina single-end flow cell. Sequencing of libraries was performed on Illumina HiSeq 2500v4 high-throughput sequencer. Fastq read files were trimmed using Cutadapt (Martin, 2011). The trimmed reads were mapped to mm10 mouse genome using HISAT2 (Kim et al., 2019). Peak calling was conducted by HOMER program run in factor mode (false discovery rate < 0.001). The intergenic peaks nearest a TSS were annotated as the corresponding gene, and peaks within a gene were further categorized into exonic, intronic, 3' or 5' untranslated regions using HOMER mm10 annotation. Venn diagrams were generated from DEG lists using InteractiVenn (<http://www.interactivenet.net>; Heberle et al., 2015).

#### Fluidigm qRT-PCR

Fluidigm qRT-PCR analysis was performed using previously published protocols (Hernandez et al., 2020; Pietras et al., 2016; Rabe et al., 2020). Pools of 100 cells were sorted directly into a 96-well PCR plate (AB2396; Thermo Fisher Scientific) containing 5  $\mu$ l of 2 $\times$  CellsDirect Reaction Mix (Invitrogen). Immediately following sort, the plate was sealed, centrifuged at 500  $\times$ g for 5 min, snap frozen, and stored at -80°C. cDNA was generated from RNA by reverse transcription using Superscript III Taq polymerase (Invitrogen) and preamplified with a custom 96-target DeltaGene (Fluidigm) primer set for 18 cycles on a thermocycler (Eppendorf). Any excess primers from the preamplification reaction were removed by Exonuclease-I (New England Biolabs) incubation, and samples were diluted in DNA

suspension buffer (Teknova) before chip loading. A Fluidigm 96.96 Dynamic Array integrated fluidics circuit was loaded with cDNA, primers, and SsoFast Sybr Green Master Mix (BioRad) and analyzed on a BioMark HD system (Fluidigm). Subsequently, data were analyzed using Fluidigm Gene Expression Software and all values were normalized to *Gusb*. The  $\Delta\Delta C_t$  approach was used to identify relative changes in gene expression. Hierarchical clustering and principal component analyses of normalized expression data were performed using ClustVis (<https://biit.cs.ut.ee/clustvis>; Metsalu and Vilo, 2015). A complete list of qRT-PCR primers included in the custom primer sets as well as their sequences can be found in Table S6. Primer sets for *Hes1*, *Hoxa2*, *Hmga1*, *Ms4a3*, *Lcn2*, and *Sod2* performed poorly due to low expression levels in HSC<sup>LT</sup>, and resulting data were not included in downstream analyses.

#### Statistical analysis

Statistical analyses were performed using Prism software (GraphPad). For RNA-seq, deSeq2 was used. Means and SD are reported except where noted. In figure legends, *n* refers to the number of biological replicates. The number of independent experiments from which the replicates derive is also reported. Except for RNA-seq and ChIP-seq analyses, statistical significance was determined by Student's *t* test or Mann-Whitney *U* test (bivariate comparisons) or one-way ANOVA with Tukey's test (multivariate comparisons).

#### Data availability

Sequencing data from this study are publicly available from the National Center for Biotechnology Information GEO accession no. GSE165810. Other datasets generated during the current study are available from the corresponding author upon reasonable request. Any data supporting the findings of this study are available from the corresponding author upon reasonable request.

#### Online supplemental material

Fig. S1, related to Figs. 1, 2, and 3, shows additional analyses and Fluidigm qRT-PCR array validation of RNA-seq data, representative FACS gating for HSC<sup>LT</sup> and characterization of Myc and puro incorporation in HSCs and MPP, and representative FACS gating and controls for *H2B-GFP* and *GFP-Myc::PU.1-EYFP* mice. Fig. S2, related to Fig. 3, contains independent validation of Myc expression changes in PU.1<sup>hi</sup> SLAM cells, as well as additional characterization of PU.1<sup>hi</sup> and PU.1<sup>lo</sup> SLAM cells after acute (1 d) and chronic (20 d) IL-1 treatment. Fig. S3, related to Fig. 4, shows division kinetics of *PU.1-ERT* HSC<sup>LT</sup> and further characterization of HSC<sup>LT</sup> cultured with IL-1. Fig. S4, related to Fig. 5, shows further characterization of PU.1 ChIP-seq datasets, *MYC* luciferase reporter assay, and characterization of Myc and cell cycle activity in PU-ER cells. Fig. S5, related to Figs. 6 and 7, shows additional characterization of *PU.1<sup>KI/KI</sup>* HSC<sup>LT</sup> after acute IL-1 challenge, independent in vivo validation of *PU.1<sup>KI/KI</sup>* results using *SCL-CreER<sup>T</sup>*-driven *PU.1* conditional knockout mice, and competitive cell culture analysis of *PU.1<sup>KI/KI</sup>* HSC<sup>LT</sup>. Table S1 provides the list of DEGs in SLAM cells from mice treated with or without IL-1 $\beta$  for 20 d. Table S2 provides GO categories, IPA

upstream regulator categories, and GSEA enrichment analysis of DEGs in SLAM cells from mice treated with or without IL-1 $\beta$  for 20 d. Table S3 provides overlaps between IL-1 downregulated genes and public datasets. Table S4 provides PU.1 ChIP-seq peak locations, scores, and PU.1/Myc motif scores. Table S5 provides GO categories of genes enriched in PU.1 ChIP-seq peak locations. Table S6 provides a list of antibodies and primers used in this study.

## Acknowledgments

We thank Garrett Hedlund for expert assistance with flow cytometry resources. We also thank the University of Colorado Office of Laboratory Animal Resources for expert vivarium administration and assistance with animal procedures.

This work was supported by National Institutes of Health grants R01 DK119394 and K01 DK098315, the Boettcher Webb-Waring Early Career Investigator Award, and the Cleo Meador and George Ryland Scott Endowed Chair in Hematology (E.M. Pietras); National Institutes of Health grant R01 AG067584 (J. DeGregori); National Institutes of Health grant F31 HL138754 (J.L. Rabe); National Institutes of Health grants F30 CA210383 and T32 AG000279 (K.C. Higa); Swiss National Science Foundation grant 179490 (T. Schroeder); and the National Science Foundation Graduate Research Fellowship Program (T.S. Mills). This work was supported in part by the University of Colorado Cancer Center Flow Cytometry Shared Resource, funded by National Cancer Institute grant P30 CA046934.

Author contributions: Conceptualization: E.M. Pietras; methodology: E.M. Pietras, J. DeGregori, D. Loeffler, K.C. Higa, and T. Schroeder; formal analysis: D. Loeffler, N. Ahmed, H. Kim, J.R. Myers, and B.M. Stevens; investigation: J.S. Chavez, J.L. Rabe, D. Loeffler, G. Hernandez, R.L. Gessner, K.E. Niño, Z. Ke, T.S. Mills, K.C. Higa, N. Ahmed, B.M. Idler, and E.M. Pietras; resources: H. Nakajima, T. Schroeder, P. Davizon-Castillo, and R.S. Welner; writing – original draft: E.M. Pietras and J.S. Chavez; writing – review and editing: E.M. Pietras, J.S. Chavez, and J. DeGregori; supervision: E.M. Pietras, J. DeGregori, C.T. Jordan, J. Ashton, and T. Schroeder; funding acquisition: E.M. Pietras and J. DeGregori.

Disclosures: The authors declare no competing interests exist.

Submitted: 5 June 2020

Revised: 1 February 2021

Accepted: 17 March 2021

## References

Ågerstam, H., N. Hansen, S. von Palffy, C. Sandén, K. Reckzeh, C. Karlsson, H. Lilljebjörn, N. Landberg, M. Askmyr, C. Högborg, et al. 2016. IL1RAP antibodies block IL-1-induced expansion of candidate CML stem cells and mediate cell killing in xenograft models. *Blood*. 128:2683–2693. <https://doi.org/10.1182/blood-2015-11-679985>

Anderson, L.A., R.M. Pfeiffer, O. Landgren, S. Gadalla, S.I. Berndt, and E.A. Engels. 2009. Risks of myeloid malignancies in patients with autoimmune conditions. *Br. J. Cancer*. 100:822–828. <https://doi.org/10.1038/sj.bjc.6604935>

Askmyr, M., H. Ågerstam, N. Hansen, S. Gordon, A. Arvanitakis, M. Rissler, G. Juliusson, J. Richter, M. Järås, and T. Fioretos. 2013. Selective killing

of candidate AML stem cells by antibody targeting of IL1RAP. *Blood*. 121:3709–3713. <https://doi.org/10.1182/blood-2012-09-458935>

Barreyro, L., B. Will, B. Bartholdy, L. Zhou, T.I. Todorova, R.F. Stanley, S. Ben-Neriah, C. Montagna, S. Parekh, A. Pellagatti, et al. 2012. Overexpression of IL-1 receptor accessory protein in stem and progenitor cells and outcome correlation in AML and MDS. *Blood*. 120:1290–1298. <https://doi.org/10.1182/blood-2012-01-404699>

Barreyro, L., T.M. Chlon, and D.T. Starczynowski. 2018. Chronic immune response dysregulation in MDS pathogenesis. *Blood*. 132:1553–1560. <https://doi.org/10.1182/blood-2018-03-784116>

Bujanover, N., O. Goldstein, Y. Greenshpan, H. Turgeman, A. Klainberger, Y. Scharff, and R. Gazit. 2018. Identification of immune-activated hematopoietic stem cells. *Leukemia*. 32:2016–2020. <https://doi.org/10.1038/s41375-018-0220-z>

Cain, D.W., P.B. Snowden, G.D. Sempowski, and G. Kelsoe. 2011. Inflammation triggers emergency granulopoiesis through a density-dependent feedback mechanism. *PLoS One*. 6:e19957. <https://doi.org/10.1371/journal.pone.0019957>

Carey, A., D.K. Edwards V, C.A. Eide, L. Newell, E. Traer, B.C. Medeiros, D.A. Pollyea, M.W. Deininger, R.H. Collins, J.W. Tyner, et al. 2017. Identification of Interleukin-1 by Functional Screening as a Key Mediator of Cellular Expansion and Disease Progression in Acute Myeloid Leukemia. *Cell Rep*. 18:3204–3218. <https://doi.org/10.1016/j.celrep.2017.03.018>

Chapple, R.H., T. Hu, Y.J. Tseng, L. Liu, A. Kitano, V. Luu, K.A. Hoegenauer, T. Iwawaki, Q. Li, and D. Nakada. 2018. ER $\alpha$  promotes murine hematopoietic regeneration through the Irela-mediated unfolded protein response. *eLife*. 7:e31159. <https://doi.org/10.7554/eLife.31159>

Delestré, L., H. Cui, M. Esposito, C. Quiveron, E. Mylonas, V. Penard-Lacroix, O. Bischof, and C. Guillouf. 2017. Senescence is a Spil-induced anti-proliferative mechanism in primary hematopoietic cells. *Haematologica*. 102:1850–1860. <https://doi.org/10.3324/haematol.2016.157636>

Dinarello, C.A. 2018. Overview of the IL-1 family in innate inflammation and acquired immunity. *Immunol. Rev*. 281:8–27. <https://doi.org/10.1111/imr.12621>

Ehninger, A., T. Boch, H. Uckelmann, M.A. Essers, K. Müdder, B.P. Sleckman, and A. Trumpp. 2014. Posttranscriptional regulation of c-Myc expression in adult murine HSCs during homeostasis and interferon- $\alpha$ -induced stress response. *Blood*. 123:3909–3913. <https://doi.org/10.1182/blood-2013-10-531038>

Essers, M.A., S. Offner, W.E. Blanco-Bose, Z. Waibler, U. Kalinke, M.A. Duchosal, and A. Trumpp. 2009. IFN $\alpha$  activates dormant haematopoietic stem cells in vivo. *Nature*. 458:904–908. <https://doi.org/10.1038/nature07815>

Etzrodt, M., N. Ahmed, P.S. Hoppe, D. Loeffler, S. Skylaki, O. Hilsenbeck, K.D. Kokkaliaris, H.M. Kaltenbach, J. Stelling, C. Nerlov, and T. Schroeder. 2019. Inflammatory signals directly instruct PU.1 in HSCs via TNF. *Blood*. 133:816–819. <https://doi.org/10.1182/blood-2018-02-832998>

Ezaki, K., M. Tsuzuki, I. Katsuta, F. Maruyama, H. Kojima, M. Okamoto, T. Nomura, M. Wakita, H. Miyazaki, R. Sobue, et al. 1995. Interleukin-1 beta (IL-1 beta) and acute leukemia: in vitro proliferative response to IL-1 beta, IL-1 beta content of leukemic cells and treatment outcome. *Leuk. Res*. 19:35–41. [https://doi.org/10.1016/0145-2126\(94\)00064-H](https://doi.org/10.1016/0145-2126(94)00064-H)

Foudi, A., K. Hochedlinger, D. Van Buren, J.W. Schindler, R. Jaenisch, V. Carey, and H. Hock. 2009. Analysis of histone 2B-GFP retention reveals slowly cycling hematopoietic stem cells. *Nat. Biotechnol*. 27:84–90. <https://doi.org/10.1038/nbt.1517>

Freire, P.R., and O.M. Conneely. 2018. NR4A1 and NR4A3 restrict HSC proliferation via reciprocal regulation of C/EBP $\alpha$  and inflammatory signaling. *Blood*. 131:1081–1093. <https://doi.org/10.1182/blood-2017-07-795757>

Fukuchi, Y., M. Ito, F. Shibata, T. Kitamura, and H. Nakajima. 2008. Activation of CCAAT/enhancer-binding protein alpha or PU.1 in hematopoietic stem cells leads to their reduced self-renewal and proliferation. *Stem Cells*. 26:3172–3181. <https://doi.org/10.1634/stemcells.2008-0320>

Gañán-Gómez, I., Y. Wei, D.T. Starczynowski, S. Colla, H. Yang, M. Cabrero-Calvo, Z.S. Bohannon, A. Verma, U. Steidl, and G. Garcia-Manero. 2015. Deregulation of innate immune and inflammatory signaling in myelodysplastic syndromes. *Leukemia*. 29:1458–1469. <https://doi.org/10.1038/leu.2015.69>

Gandhi, V., W. Plunkett, and J.E. Cortes. 2014. Omacetaxine: a protein translation inhibitor for treatment of chronic myelogenous leukemia. *Clin. Cancer Res*. 20:1735–1740. <https://doi.org/10.1158/1078-0432.CCR-13-1283>

Gerloff, D., R. Grundler, A.A. Wurm, D. Bräuer-Hartmann, C. Katzerke, J.U. Hartmann, V. Madan, C. Müller-Tidow, J. Duyster, D.G. Tenen, et al.



2015. NF- $\kappa$ B/STAT5/miR-155 network targets PU.1 in FLT3-ITD-driven acute myeloid leukemia. *Leukemia*. 29:535–547. <https://doi.org/10.1038/leu.2014.231>
- Göthert, J.R., S.E. Gustin, M.A. Hall, A.R. Green, B. Göttgens, D.J. Izon, and C.G. Begley. 2005. In vivo fate-tracing studies using the Scl stem cell enhancer: embryonic hematopoietic stem cells significantly contribute to adult hematopoiesis. *Blood*. 105:2724–2732. <https://doi.org/10.1182/blood-2004-08-3037>
- Haas, S., J. Hansson, D. Klimmeck, D. Loeffler, L. Velten, H. Uckelmann, S. Wurzer, A.M. Prendergast, A. Schnell, K. Hexel, et al. 2015. Inflammation-Induced Emergency Megakaryopoiesis Driven by Hematopoietic Stem Cell-like Megakaryocyte Progenitors. *Cell Stem Cell*. 17:422–434. <https://doi.org/10.1016/j.stem.2015.07.007>
- Harrison, D.E., and C.P. Lerner. 1991. Most primitive hematopoietic stem cells are stimulated to cycle rapidly after treatment with 5-fluorouracil. *Blood*. 78:1237–1240. <https://doi.org/10.1182/blood.V78.5.1237.1237>
- Heberle, H., G.V. Meirelles, F.R. da Silva, G.P. Telles, and R. Minghim. 2015. InteractiVenn: a web-based tool for the analysis of sets through Venn diagrams. *BMC Bioinformatics*. 16:169. <https://doi.org/10.1186/s12859-015-0611-3>
- Heidt, T., H.B. Sager, G. Courties, P. Dutta, Y. Iwamoto, A. Zaltsman, C. von Zur Muhlen, C. Bode, G.L. Frichione, J. Denninger, et al. 2014. Chronic variable stress activates hematopoietic stem cells. *Nat. Med.* 20:754–758. <https://doi.org/10.1038/nm.3589>
- Heinz, S., C. Benner, N. Spann, E. Bertolino, Y.C. Lin, P. Laslo, J.X. Cheng, C. Murre, H. Singh, and C.K. Glass. 2010. Simple combinations of lineage-determining transcription factors prime cis-regulatory elements required for macrophage and B cell identities. *Mol. Cell*. 38:576–589. <https://doi.org/10.1016/j.molcel.2010.05.004>
- Hemmati, S., T. Sinclair, M. Tong, B. Bartholdy, R.O. Okabe, K. Ames, L. Ostrodka, T. Haque, I. Kaur, T.S. Mills, et al. 2019. PI3 kinase alpha and delta promote hematopoietic stem cell activation. *JCI Insight*. 4:e125832. <https://doi.org/10.1172/jci.insight.125832>
- Henry, C.J., M. Casás-Selves, J. Kim, V. Zaberezhnyy, L. Aghili, A.E. Daniel, L. Jimenez, T. Azam, E.N. McNamee, E.T. Clambey, et al. 2015. Aging-associated inflammation promotes selection for adaptive oncogenic events in B cell progenitors. *J. Clin. Invest.* 125:4666–4680. <https://doi.org/10.1172/JCI83024>
- Hernandez, G., T.S. Mills, J.L. Rabe, J.S. Chavez, S. Kuldaneck, G. Kirkpatrick, L. Noetzli, W.K. Jubair, M. Zanche, J.R. Myers, et al. 2020. Pro-inflammatory cytokine blockade attenuates myeloid expansion in a murine model of rheumatoid arthritis. *Haematologica*. 105:585–597. <https://doi.org/10.3324/haematol.2018.197210>
- Hilsenbeck, O., M. Schwarzfischer, S. Skylaki, B. Schauburger, P.S. Hoppe, D. Loeffler, K.D. Kokkalis, S. Hastreiter, E. Skylaki, A. Filipczyk, et al. 2016. Software tools for single-cell tracking and quantification of cellular and molecular properties. *Nat. Biotechnol.* 34:703–706. <https://doi.org/10.1038/nbt.3626>
- Higa, K.C., A. Goodspeed, J.S. Chavez, M. De Dominicis, E.P. Danis, V. Zaberezhnyy, J.L. Rabe, D.G. Tenen, E.M. Pietras, and J. DeGregori. 2021. Chronic Interleukin-1 triggers selection for Cebpa-knockout multipotent hematopoietic progenitors. *J. Exp. Med.* In press. <https://doi.org/10.1084/jem.20200560>
- Hilsenbeck, O., M. Schwarzfischer, D. Loeffler, S. Dimopoulos, S. Hastreiter, C. Marr, F.J. Theis, and T. Schroeder. 2017. fastER: a user-friendly tool for ultrafast and robust cell segmentation in large-scale microscopy. *Bioinformatics*. 33:2020–2028. <https://doi.org/10.1093/bioinformatics/btx107>
- Hinge, A., J. He, J. Bartram, J. Javier, J. Xu, E. Fjellman, H. Sesaki, T. Li, J. Yu, M. Wunderlich, et al. 2020. Asymmetrically Segregated Mitochondria Provide Cellular Memory of Hematopoietic Stem Cell Replicative History and Drive HSC Attrition. *Cell Stem Cell*. 26:420–430.e6. <https://doi.org/10.1016/j.stem.2020.01.016>
- Hock, H., M.J. Hamblen, H.M. Rooke, J.W. Schindler, S. Saleque, Y. Fujiwara, and S.H. Orkin. 2004. Gfi-1 restricts proliferation and preserves functional integrity of haematopoietic stem cells. *Nature*. 431:1002–1007. <https://doi.org/10.1038/nature02994>
- Hoppe, P.S., M. Schwarzfischer, D. Loeffler, K.D. Kokkalis, O. Hilsenbeck, N. Moritz, M. Endeale, A. Filipczyk, A. Gambardella, N. Ahmed, et al. 2016. Early myeloid lineage choice is not initiated by random PU.1 to GATA1 protein ratios. *Nature*. 535:299–302. <https://doi.org/10.1038/nature18320>
- Hosokawa, H., J. Ungerback, X. Wang, M. Matsumoto, K.I. Nakayama, S.M. Cohen, T. Tanaka, and E.V. Rothenberg. 2018. Transcription Factor PU.1 Represses and Activates Gene Expression in Early T Cells by Redirecting Partner Transcription Factor Binding. *Immunity*. 48:1119–1134.e7. <https://doi.org/10.1016/j.immuni.2018.04.024>
- Huang, C.Y., A.L. Bredemeyer, L.M. Walker, C.H. Bassing, and B.P. Sleckman. 2008. Dynamic regulation of c-Myc proto-oncogene expression during lymphocyte development revealed by a GFP-c-Myc knock-in mouse. *Eur. J. Immunol.* 38:342–349. <https://doi.org/10.1002/eji.200737972>
- Huang, W., B.T. Sherman, and R.A. Lempicki. 2009. Systematic and integrative analysis of large gene lists using DAVID bioinformatics resources. *Nat. Protoc.* 4:44–57. <https://doi.org/10.1038/nprot.2008.211>
- Iritani, B.M., and R.N. Eisenman. 1999. c-Myc enhances protein synthesis and cell size during B lymphocyte development. *Proc. Natl. Acad. Sci. USA*. 96:13180–13185. <https://doi.org/10.1073/pnas.96.23.13180>
- Jalbert, E., and E.M. Pietras. 2018. Analysis of Murine Hematopoietic Stem Cell Proliferation During Inflammation. *Methods Mol. Biol.* 1686:183–200. [https://doi.org/10.1007/978-1-4939-7371-2\\_14](https://doi.org/10.1007/978-1-4939-7371-2_14)
- Kaasinen, E., O. Kuismin, K. Rajamäki, H. Ristolainen, M. Avikko, J. Kondein, S. Saarinen, D.G. Berta, R. Katainen, E.A.M. Hirvonen, et al. 2019. Impact of constitutional TET2 haploinsufficiency on molecular and clinical phenotype in humans. *Nat. Commun.* 10:1252. <https://doi.org/10.1038/s41467-019-09198-7>
- Kihara-Negishi, F., H. Yamamoto, M. Suzuki, T. Yamada, T. Sakurai, T. Tamura, and T. Oikawa. 2001. In vivo complex formation of PU.1 with HDAC1 associated with PU.1-mediated transcriptional repression. *Oncogene*. 20:6039–6047. <https://doi.org/10.1038/sj.onc.1204756>
- Kim, D., J.M. Paggi, C. Park, C. Bennett, and S.L. Salzberg. 2019. Graph-based genome alignment and genotyping with HISAT2 and HISAT-genotype. *Nat. Biotechnol.* 37:907–915. <https://doi.org/10.1038/s41587-019-0201-4>
- King, K.Y., and M.A. Goodell. 2011. Inflammatory modulation of HSCs: viewing the HSC as a foundation for the immune response. *Nat. Rev. Immunol.* 11:685–692. <https://doi.org/10.1038/nri3062>
- King, K.Y., M.T. Baldrige, D.C. Weksberg, S.M. Chambers, G.L. Lukov, S. Wu, N.C. Boles, S.Y. Jung, J. Qin, D. Liu, et al. 2011. Irgm1 protects hematopoietic stem cells by negative regulation of IFN signaling. *Blood*. 118:1525–1533. <https://doi.org/10.1182/blood-2011-01-328682>
- Kirstetter, P., K. Anderson, B.T. Porse, S.E. Jacobsen, and C. Nerlov. 2006. Activation of the canonical Wnt pathway leads to loss of hematopoietic stem cell repopulation and multilineage differentiation block. *Nat. Immunol.* 7:1048–1056. <https://doi.org/10.1038/ni1381>
- Kueh, H.Y., A. Champhekar, S.L. Nutt, M.B. Elowitz, and E.V. Rothenberg. 2013. Positive feedback between PU.1 and the cell cycle controls myeloid differentiation. *Science*. 341:670–673. <https://doi.org/10.1126/science.1240831>
- Laberge, R.M., Y. Sun, A.V. Orjalo, C.K. Patil, A. Freund, L. Zhou, S.C. Curran, A.R. Davalos, K.A. Wilson-Edell, S. Liu, et al. 2015. MTOR regulates the pro-tumorigenic senescence-associated secretory phenotype by promoting IL1A translation. *Nat. Cell Biol.* 17:1049–1061. <https://doi.org/10.1038/ncb3195>
- Laconi, E., F. Marongiu, and J. DeGregori. 2020. Cancer as a disease of old age: changing mutational and microenvironmental landscapes. *Br. J. Cancer*. 122:943–952. <https://doi.org/10.1038/s41416-019-0721-1>
- Laurenti, E., B. Varnum-Finney, A. Wilson, I. Ferrero, W.E. Blanco-Bose, A. Ehninger, P.S. Knoepfler, P.F. Cheng, H.R. MacDonald, R.N. Eisenman, et al. 2008. Hematopoietic stem cell function and survival depend on c-Myc and N-Myc activity. *Cell Stem Cell*. 3:611–624. <https://doi.org/10.1016/j.stem.2008.09.005>
- Li, M.M., M.R. MacDonald, and C.M. Rice. 2015. To translate, or not to translate: viral and host mRNA regulation by interferon-stimulated genes. *Trends Cell Biol.* 25:320–329. <https://doi.org/10.1016/j.tcb.2015.02.001>
- Liang, R., T. Arif, S. Kalmykova, A. Kasianov, M. Lin, V. Menon, J. Qiu, J.M. Bernitz, K. Moore, F. Lin, et al. 2020. Restraining Lysosomal Activity Preserves Hematopoietic Stem Cell Quiescence and Potency. *Cell Stem Cell*. 26:359–376.e7. <https://doi.org/10.1016/j.stem.2020.01.013>
- Loeffler, D., W. Wang, A. Hopf, O. Hilsenbeck, P.E. Bourging, F. Rudolf, I. Martin, and T. Schroeder. 2018. Mouse and human HSPC immobilization in liquid culture by CD43- or CD44-antibody coating. *Blood*. 131:1425–1429. <https://doi.org/10.1182/blood-2017-07-794131>
- Martin, M. 2011. Cutadapt removes adapter sequences from high-throughput sequencing reads. *EMBnet journal*. 17:10–12. <https://doi.org/10.14806/ej.17.1.200>
- Matatal, K.A., M. Jeong, S. Chen, D. Sun, F. Chen, Q. Mo, M. Kimmel, and K.Y. King. 2016. Chronic Infection Depletes Hematopoietic Stem Cells through Stress-Induced Terminal Differentiation. *Cell Rep.* 17:2584–2595. <https://doi.org/10.1016/j.celrep.2016.11.031>
- Matatal, K.A., C.S. Kadmon, and K.Y. King. 2018. Detecting Hematopoietic Stem Cell Proliferation Using BrdU Incorporation. *Methods Mol. Biol.* 1686:91–103. [https://doi.org/10.1007/978-1-4939-7371-2\\_7](https://doi.org/10.1007/978-1-4939-7371-2_7)



- Matsumoto, A., S. Takeishi, T. Kanie, E. Susaki, I. Onoyama, Y. Tateishi, K. Nakayama, and K.I. Nakayama. 2011. p57 is required for quiescence and maintenance of adult hematopoietic stem cells. *Cell Stem Cell*. 9:262–271. <https://doi.org/10.1016/j.stem.2011.06.014>
- McKenzie, M.D., M. Ghisi, E.P. Oxley, S. Ngo, L. Cimmino, C. Esnault, R. Liu, J.M. Salmon, C.C. Bell, N. Ahmed, et al. 2019. Interconversion between Tumorigenic and Differentiated States in Acute Myeloid Leukemia. *Cell Stem Cell*. 25:258–272.e9. <https://doi.org/10.1016/j.stem.2019.07.001>
- Metsalu, T., and J. Vilo. 2015. ClustVis: a web tool for visualizing clustering of multivariate data using Principal Component Analysis and heatmap. *Nucleic Acids Res.* 43(W1):W566–W570. <https://doi.org/10.1093/nar/gkv468>
- Mitchell, K., L. Barreyro, T.I. Todorova, S.J. Taylor, I. Antony-Debré, S.R. Narayanagari, L.A. Carvajal, J. Leite, Z. Piperdi, G. Pendurti, et al. 2018. IL1RAP potentiates multiple oncogenic signaling pathways in AML. *J. Exp. Med.* 215:1709–1727. <https://doi.org/10.1084/jem.20180147>
- Morrison, S.J., and D.T. Scadden. 2014. The bone marrow niche for haematopoietic stem cells. *Nature*. 505:327–334. <https://doi.org/10.1038/nature12984>
- Mueller, B.U., T. Pabst, J. Fos, V. Petkovic, M.F. Fey, N. Asou, U. Buerger, and D.G. Tenen. 2006. ATRA resolves the differentiation block in t(15;17) acute myeloid leukemia by restoring PU.1 expression. *Blood*. 107:3330–3338. <https://doi.org/10.1182/blood-2005-07-3068>
- Muto, T., C.S. Walker, K. Choi, K. Hueneman, M.A. Smith, Z. Gul, G. Garcia-Manero, A. Ma, Y. Zheng, and D.T. Starczynowski. 2020. Adaptive response to inflammation contributes to sustained myelopoiesis and confers a competitive advantage in myelodysplastic syndrome HSCs. *Nat. Immunol.* 21:535–545. <https://doi.org/10.1038/s41590-020-0663-z>
- Noguera, N.I., M.L. Piredda, R. Tauli, G. Catalano, G. Angelini, G. Gaur, C. Nervi, M.T. Voso, A. Lunardi, P.P. Pandolfi, and F. Lo-Coco. 2016. PML/RARa inhibits PTEN expression in hematopoietic cells by competing with PU.1 transcriptional activity. *Oncotarget*. 7:66386–66397. <https://doi.org/10.18632/oncotarget.11964>
- Oikawa, T., T. Yamada, F. Kihara-Negishi, H. Yamamoto, N. Kondoh, Y. Hitomi, and Y. Hashimoto. 1999. The role of Ets family transcription factor PU.1 in hematopoietic cell differentiation, proliferation and apoptosis. *Cell Death Differ.* 6:599–608. <https://doi.org/10.1038/sj.cdd.4400534>
- Peng, T., K. Thorn, T. Schroeder, L. Wang, F.J. Theis, C. Marr, and N. Navab. 2017. A BaSiC tool for background and shading correction of optical microscopy images. *Nat. Commun.* 8:14836. <https://doi.org/10.1038/ncomms14836>
- Pietras, E.M. 2017. Inflammation: a key regulator of hematopoietic stem cell fate in health and disease. *Blood*. 130:1693–1698. <https://doi.org/10.1182/blood-2017-06-780882>
- Pietras, E.M., M.R. Warr, and E. Passegué. 2011. Cell cycle regulation in hematopoietic stem cells. *J. Cell Biol.* 195:709–720. <https://doi.org/10.1083/jcb.201102131>
- Pietras, E.M., R. Lakshminarasimhan, J.M. Techner, S. Fong, J. Flach, M. Binnewies, and E. Passegué. 2014. Re-entry into quiescence protects hematopoietic stem cells from the killing effect of chronic exposure to type I interferons. *J. Exp. Med.* 211:245–262. <https://doi.org/10.1084/jem.20131043>
- Pietras, E.M., C. Mirantes-Barbeito, S. Fong, D. Loeffler, L.V. Kovtonyuk, S. Zhang, R. Lakshminarasimhan, C.P. Chin, J.M. Techner, B. Will, et al. 2016. Chronic interleukin-1 exposure drives haematopoietic stem cells towards precocious myeloid differentiation at the expense of self-renewal. *Nat. Cell Biol.* 18:607–618. <https://doi.org/10.1038/ncb3346>
- Polymenis, M., and R. Aramayo. 2015. Translate to divide: control of the cell cycle by protein synthesis. *Microb. Cell*. 2:94–104. <https://doi.org/10.15698/mic2015.04.198>
- Porse, B.T., D. Bryder, K. Theilgaard-Mönch, M.S. Hasemann, K. Anderson, I. Damgaard, S.E. Jacobsen, and C. Nerlov. 2005. Loss of C/EBP alpha cell cycle control increases myeloid progenitor proliferation and transforms the neutrophil granulocyte lineage. *J. Exp. Med.* 202:85–96. <https://doi.org/10.1084/jem.20050067>
- Porter, S.N., A.S. Cluster, R.A.J. Signer, J. Voigtmann, D.A. Monlish, L.G. Schuettelpelz, and J.A. Magee. 2016. Pten Cell Autonomously Modulates the Hematopoietic Stem Cell Response to Inflammatory Cytokines. *Stem Cell Reports*. 6:806–814. <https://doi.org/10.1016/j.stemcr.2016.04.008>
- Prendergast, A.M., and M.A. Essers. 2014. Hematopoietic stem cells, infection, and the niche. *Ann. N. Y. Acad. Sci.* 1310:51–57. <https://doi.org/10.1111/nyas.12400>
- Pronk, C.J., D.J. Rossi, R. Månsson, J.L. Attema, G.L. Norddahl, C.K. Chan, M. Sigvardsson, I.L. Weissman, and D. Bryder. 2007. Elucidation of the phenotypic, functional, and molecular topography of a myeloerythroid progenitor cell hierarchy. *Cell Stem Cell*. 1:428–442. <https://doi.org/10.1016/j.stem.2007.07.005>
- Pulikkan, J.A., D.G. Tenen, and G. Behre. 2017. C/EBPα deregulation as a paradigm for leukemogenesis. *Leukemia*. 31:2279–2285. <https://doi.org/10.1038/leu.2017.229>
- Rabe, J.L., G. Hernandez, J.S. Chavez, T.S. Mills, C. Nerlov, and E.M. Pietras. 2020. CD34 and EPCR coordinately enrich functional murine hematopoietic stem cells under normal and inflammatory conditions. *Exp. Hematol.* 81:1–15.e6. <https://doi.org/10.1016/j.exphem.2019.12.003>
- Rhyasen, G.W., L. Bolanos, J. Fang, A. Jerez, M. Wunderlich, C. Rigolino, L. Mathews, M. Ferrer, N. Southall, R. Guha, et al. 2013. Targeting IRAK1 as a therapeutic approach for myelodysplastic syndrome. *Cancer Cell*. 24:90–104. <https://doi.org/10.1016/j.ccr.2013.05.006>
- Rodgers, J.T., K.Y. King, J.O. Brett, M.J. Cromie, G.W. Charville, K.K. Maguire, C. Brunson, N. Mastey, L. Liu, C.R. Tsai, et al. 2014. mTORC1 controls the adaptive transition of quiescent stem cells from G0 to G(Alert). *Nature*. 510:393–396. <https://doi.org/10.1038/nature13255>
- Rodríguez, A., K. Zhang, A. Färkkilä, J. Filiatrault, C. Yang, M. Velázquez, E. Furutani, D.C. Goldman, B. Garcia de Teresa, G. Garza-Mayén, et al. 2021. MYC Promotes Bone Marrow Stem Cell Dysfunction in Fanconi Anemia. *Cell Stem Cell*. 28:33–47.e8. <https://doi.org/10.1016/j.stem.2020.09.004>
- Rosenbauer, F., K. Wagner, J.L. Kutok, H. Iwasaki, M.M. Le Beau, Y. Okuno, K. Akashi, S. Fiering, and D.G. Tenen. 2004. Acute myeloid leukemia induced by graded reduction of a lineage-specific transcription factor, PU.1. *Nat. Genet.* 36:624–630. <https://doi.org/10.1038/ng1361>
- Säwén, P., S. Lang, P. Mandal, D.J. Rossi, S. Soneji, and D. Bryder. 2016. Mitotic History Reveals Distinct Stem Cell Populations and Their Contributions to Hematopoiesis. *Cell Rep.* 14:2809–2818. <https://doi.org/10.1016/j.celrep.2016.02.073>
- Schaefer, B.C., M.L. Schaefer, J.W. Kappler, P. Marrack, and R.M. Kedl. 2001. Observation of antigen-dependent CD8+ T-cell/ dendritic cell interactions in vivo. *Cell. Immunol.* 214:110–122. <https://doi.org/10.1006/cimm.2001.1895>
- Schuettelpelz, L.G., J.N. Borgerding, M.J. Christopher, P.K. Gopalan, M.P. Romine, A.C. Herman, J.R. Woloszynek, A.M. Greenbaum, and D.C. Link. 2014. G-CSF regulates hematopoietic stem cell activity, in part, through activation of Toll-like receptor signaling. *Leukemia*. 28:1851–1860. <https://doi.org/10.1038/leu.2014.68>
- Scognamiglio, R., N. Cabezas-Wallscheid, M.C. Thier, S. Altamura, A. Reyes, A.M. Prendergast, D. Baumgärtner, L.S. Carnevalli, A. Atzberger, S. Haas, et al. 2016. Myc Depletion Induces a Pluripotent Dormant State Mimicking Diapause. *Cell*. 164:668–680. <https://doi.org/10.1016/j.cell.2015.12.033>
- Signer, R.A., J.A. Magee, A. Salic, and S.J. Morrison. 2014. Haematopoietic stem cells require a highly regulated protein synthesis rate. *Nature*. 509:49–54. <https://doi.org/10.1038/nature13035>
- Signer, R.A., L. Qi, Z. Zhao, D. Thompson, A.A. Sigova, Z.P. Fan, G.N. DeMartino, R.A. Young, N. Sonenberg, and S.J. Morrison. 2016. The rate of protein synthesis in hematopoietic stem cells is limited partly by 4E-BPs. *Genes Dev.* 30:1698–1703. <https://doi.org/10.1101/gad.282756.116>
- Smith, M.A., G.S. Choudhary, A. Pellagatti, K. Choi, L.C. Bolanos, T.D. Bhagat, S. Gordon-Mitchell, D. Von Ahrens, K. Pradhan, V. Steeples, et al. 2019. U2AF1 mutations induce oncogenic IRAK4 isoforms and activate innate immune pathways in myeloid malignancies. *Nat. Cell Biol.* 21:640–650. <https://doi.org/10.1038/s41556-019-0314-5>
- Solomon, L.A., S. Podder, J. He, N.L. Jackson-Chornenki, K. Gibson, R.G. Ziliotto, J. Rhee, and R.P. DeKoter. 2017. Coordination of Myeloid Differentiation with Reduced Cell Cycle Progression by PU.1 Induction of MicroRNAs Targeting Cell Cycle Regulators and Lipid Anabolism. *Mol. Cell Biol.* 37:e00013-17. <https://doi.org/10.1128/MCB.00013-17>
- Staber, P.B., P. Zhang, M. Ye, R.S. Welner, C. Nombela-Arrieta, C. Bach, M. Kerenyi, B.A. Bartholdy, H. Zhang, M. Alberich-Jordá, et al. 2013. Sustained PU.1 levels balance cell-cycle regulators to prevent exhaustion of adult hematopoietic stem cells. *Mol. Cell*. 49:934–946. <https://doi.org/10.1016/j.molcel.2013.01.007>
- Stevens, B.M., N. Khan, A. D'Alessandro, T. Nemkov, A. Winters, C.L. Jones, W. Zhang, D.A. Pollyea, and C.T. Jordan. 2018. Characterization and targeting of malignant stem cells in patients with advanced myelodysplastic syndromes. *Nat. Commun.* 9:3694. <https://doi.org/10.1038/s41467-018-05984-x>
- Takizawa, H., K. Fritsch, L.V. Kovtonyuk, Y. Saito, C. Yakkala, K. Jacobs, A.K. Ahuja, M. Lopes, A. Hausmann, W.D. Hardt, et al. 2017. Pathogen-Induced TLR4-TRIF Innate Immune Signaling in Hematopoietic Stem Cells Promotes Proliferation but Reduces Competitive Fitness. *Cell Stem Cell*. 21:225–240.e5. <https://doi.org/10.1016/j.stem.2017.06.013>

- Ueda, Y., D.W. Cain, M. Kuraoka, M. Kondo, and G. Kelsoe. 2009. IL-1R type I-dependent hemopoietic stem cell proliferation is necessary for inflammatory granulopoiesis and reactive neutrophilia. *J. Immunol.* 182: 6477–6484. <https://doi.org/10.4049/jimmunol.0803961>
- Umek, R.M., A.D. Friedman, and S.L. McKnight. 1991. CCAAT-enhancer binding protein: a component of a differentiation switch. *Science.* 251: 288–292. <https://doi.org/10.1126/science.1987644>
- Vangala, R.K., M.S. Heiss-Neumann, J.S. Rangatia, S.M. Singh, C. Schoch, D.G. Tenen, W. Hiddemann, and G. Behre. 2003. The myeloid master regulator transcription factor PU.1 is inactivated by AML1-ETO in t(8;21) myeloid leukemia. *Blood.* 101:270–277. <https://doi.org/10.1182/blood-2002-04-1288>
- Walsh, J.C., R.P. DeKoter, H.J. Lee, E.D. Smith, D.W. Lancki, M.F. Gurish, D.S. Friend, R.L. Stevens, J. Anastasi, and H. Singh. 2002. Cooperative and antagonistic interplay between PU.1 and GATA-2 in the specification of myeloid cell fates. *Immunity.* 17:665–676. [https://doi.org/10.1016/S1074-7613\(02\)00452-1](https://doi.org/10.1016/S1074-7613(02)00452-1)
- Walter, D., A. Lier, A. Geiselhart, F.B. Thalheimer, S. Huntscha, M.C. Sobotta, B. Moehrl, D. Brocks, I. Bayindir, P. Kaschutnig, et al. 2015. Exit from dormancy provokes DNA-damage-induced attrition in haematopoietic stem cells. *Nature.* 520:549–552. <https://doi.org/10.1038/nature14131>
- Weisser, M., U.M. Demel, S. Stein, L. Chen-Wichmann, F. Touzot, G. Santilli, S. Sujer, C. Brendel, U. Siler, M. Cavazzana, et al. 2016. Hyperinflammation in patients with chronic granulomatous disease leads to impairment of hematopoietic stem cell functions. *J. Allergy Clin. Immunol.* 138:219–228.e9. <https://doi.org/10.1016/j.jaci.2015.11.028>
- Will, B., T.O. Vogler, S. Narayanagari, B. Bartholdy, T.I. Todorova, M. da Silva Ferreira, J. Chen, Y. Yu, J. Mayer, L. Barreiro, et al. 2015. Minimal PU.1 reduction induces a preleukemic state and promotes development of acute myeloid leukemia. *Nat. Med.* 21:1172–1181. <https://doi.org/10.1038/nm.3936>
- Wilson, A., M.J. Murphy, T. Oskarsson, K. Kaloulis, M.D. Bettess, G.M. Oser, A.C. Pasche, C. Knabenhans, H.R. Macdonald, and A. Trumpp. 2004. c-Myc controls the balance between hematopoietic stem cell self-renewal and differentiation. *Genes Dev.* 18:2747–2763. <https://doi.org/10.1101/gad.313104>
- Wilson, A., E. Laurenti, G. Oser, R.C. van der Wath, W. Blanco-Bose, M. Jaworski, S. Offner, C.F. Dunant, L. Eshkind, E. Bockamp, et al. 2008. Hematopoietic stem cells reversibly switch from dormancy to self-renewal during homeostasis and repair. *Cell.* 135:1118–1129. <https://doi.org/10.1016/j.cell.2008.10.048>
- Yamashita, M., and E. Passegué. 2019. TNF- $\alpha$  Coordinates Hematopoietic Stem Cell Survival and Myeloid Regeneration. *Cell Stem Cell.* 25: 357–372.e7. <https://doi.org/10.1016/j.stem.2019.05.019>
- Yang, H., H. Liang, J.S. Yan, R. Tao, S.G. Hao, and L.Y. Ma. 2012. Downregulation of hematopoiesis master regulator PU.1 via aberrant methylation in chronic myeloid leukemia. *Int. J. Hematol.* 96:65–73. <https://doi.org/10.1007/s12185-012-1106-x>
- Zambetti, N.A., Z. Ping, S. Chen, K.J.G. Kenswil, M.A. Mylona, M.A. Sanders, R.M. Hoogenboezem, E.M.J. Bindels, M.N. Adisty, P.M.H. Van Strien, et al. 2016. Mesenchymal Inflammation Drives Genotoxic Stress in Hematopoietic Stem Cells and Predicts Disease Evolution in Human Pre-leukemia. *Cell Stem Cell.* 19:613–627. <https://doi.org/10.1016/j.stem.2016.08.021>
- Zeng, H., R. Yücel, C. Kosan, L. Klein-Hitpass, and T. Möröy. 2004. Transcription factor Gfi1 regulates self-renewal and engraftment of hematopoietic stem cells. *EMBO J.* 23:4116–4125. <https://doi.org/10.1038/sj.emboj.7600419>
- Zhang, B., S. Chu, P. Agarwal, V.L. Campbell, L. Hopcroft, H.G. Jørgensen, A. Lin, K. Gaal, T.L. Holyoake, and R. Bhatia. 2016. Inhibition of interleukin-1 signaling enhances elimination of tyrosine kinase inhibitor-treated CML stem cells. *Blood.* 128:2671–2682. <https://doi.org/10.1182/blood-2015-11-679928>
- Zhao, M., F. Tao, A. Venkatraman, Z. Li, S.E. Smith, J. Unruh, S. Chen, C. Ward, P. Qian, J.M. Perry, et al. 2019. N-Cadherin-Expressing Bone and Marrow Stromal Progenitor Cells Maintain Reserve Hematopoietic Stem Cells. *Cell Rep.* 26:652–669.e6. <https://doi.org/10.1016/j.celrep.2018.12.093>
- Ziliotto, R., M.R. Gruca, S. Podder, G. Noel, C.K. Ogle, D.A. Hess, and R.P. DeKoter. 2014. PU.1 promotes cell cycle exit in the murine myeloid lineage associated with downregulation of E2F1. *Exp. Hematol.* 42: 204–217.e1. <https://doi.org/10.1016/j.exphem.2013.11.011>

## Supplemental material

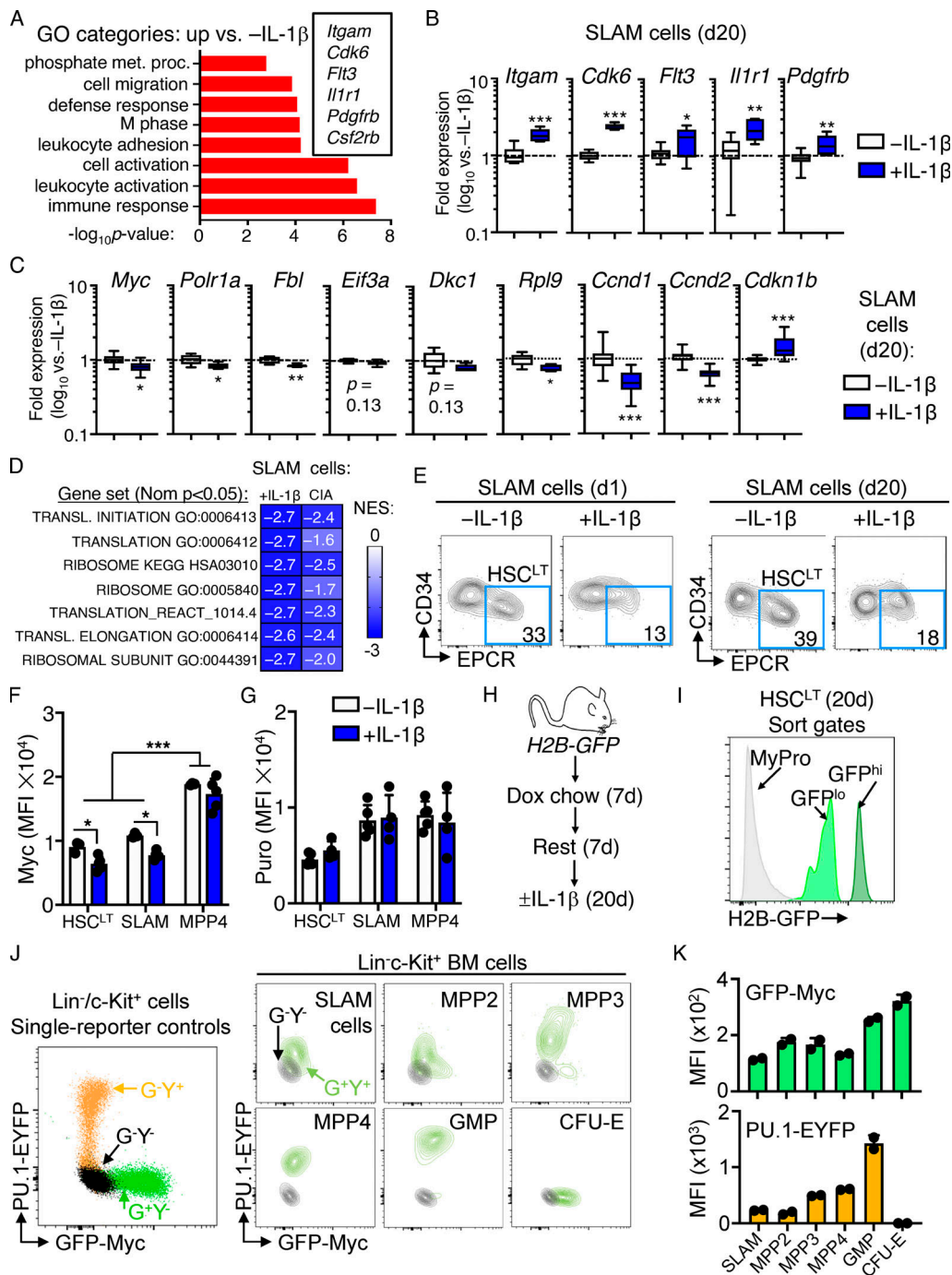


Figure S1. **Characterization of SLAM cells and reporter mice.** (A) GO category enrichment of significantly upregulated DEGs in SLAM cells from mice treated for 20 d with or without IL-1 $\beta$  versus 20 d -IL-1 $\beta$ , expressed as  $-\log_{10}$  P value. See Table S2 for complete list of GO categories. (B and C) Quantification by Fluidigm qRT-PCR array of gene expression in SLAM cells from mice treated with or without IL-1 $\beta$  for 20 d ( $n = 8$ /group). Data are expressed as  $\log_{10}$  fold expression versus -IL-1 $\beta$ . Box represents upper and lower quartiles with line representing median value. Whiskers represent minimum and maximum values. Data are representative of two independent experiments. (D) Comparison of normalized enrichment scores (NESs) for indicated gene signatures from IL-1-exposed SLAM cells and SLAM cells from CIA mice (GSE129511). (E) Representative FACS plots showing frequencies of phenotypic HSC<sup>LT</sup> fraction within the SLAM gate from mice treated with IL-1 $\beta$  versus without IL-1 $\beta$  for either 1 or 20 d. Data are representative of multiple (more than three) experiments. (F) Geometric MFI of Myc from one of three experiments ( $n = 5$ /group). Individual values are shown with bars representing mean values. (G) Geometric MFI of puro from one of three experiments ( $n = 5$ /group). Individual values are shown with bars representing mean values. (H) Experimental design for H2B-GFP in vivo labeling experiments. Dox, doxycycline. (I) Representative sort gates showing identification of GFP<sup>hi</sup> and GFP<sup>lo</sup> populations within the HSC<sup>LT</sup> gate. Myeloid progenitors (MyPro), which rapidly dilute the GFP label, are shown in gray. (J) Representative FACS plot showing GFP and YFP profiles of single-color control Lin<sup>-</sup>/c-Kit<sup>+</sup> HSPC from Myc-GFP (G<sup>+</sup>Y<sup>-</sup>) or PU.1-EYFP (G<sup>+</sup>Y<sup>+</sup>) mice relative to G<sup>-</sup>Y<sup>-</sup> controls (left) and representative FACS plots of defined HSPC populations from Myc-GFP::PU.1-EYFP (G<sup>+</sup>Y<sup>+</sup>) mice versus G<sup>-</sup>Y<sup>-</sup> controls (right). (K) Quantification of GFP and YFP levels in each HSPC population from mice in J ( $n = 2$ /group). Individual values are shown with bars representing mean values. Data in J and K are representative of at least two independent experiments. \*,  $P < 0.05$ ; \*\*,  $P < 0.01$ ; \*\*\*,  $P < 0.001$  by Mann-Whitney U test or ANOVA with Tukey's post-test in F and G. Error bars represent SD.



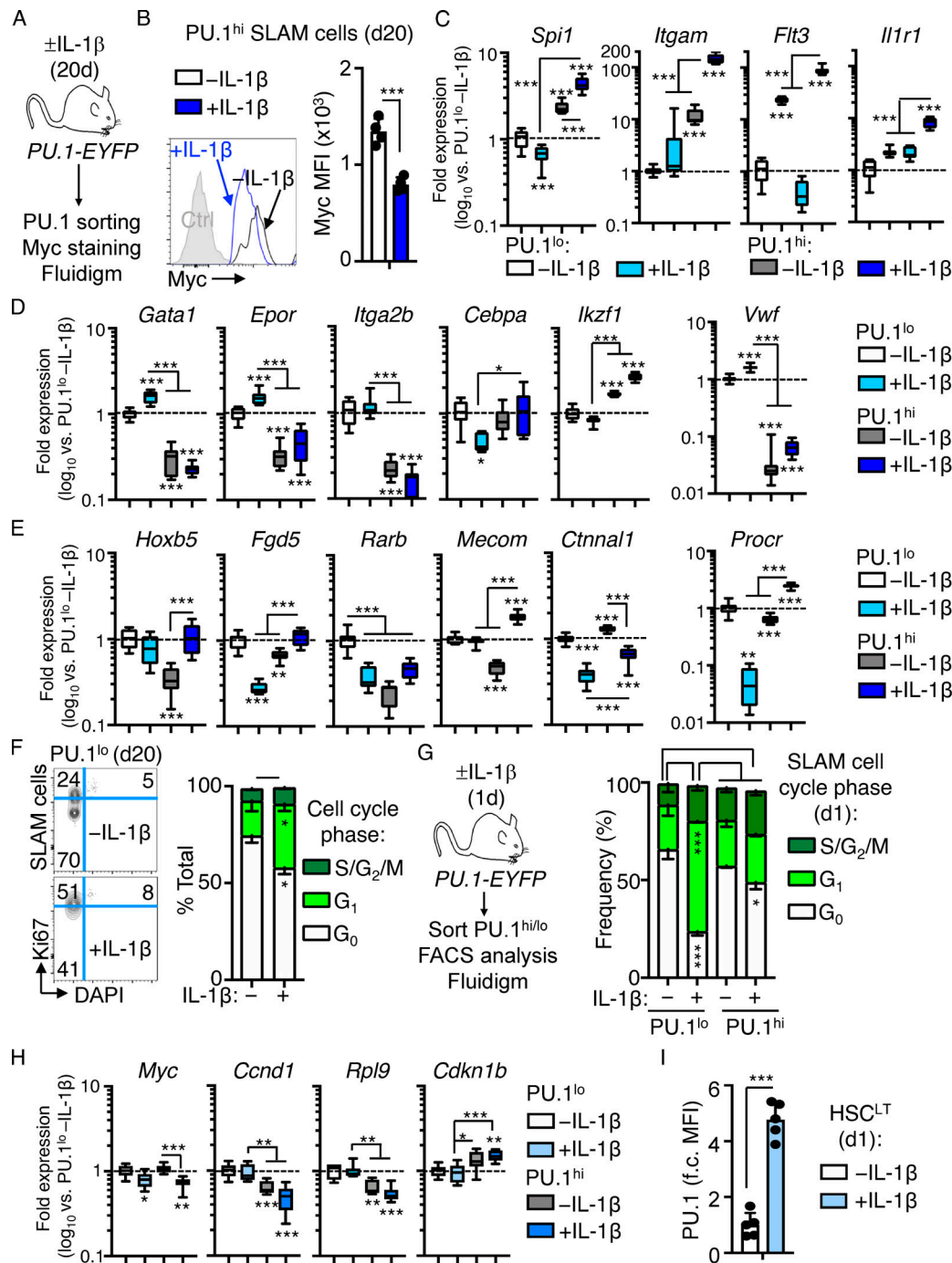


Figure S2. **Characterization of SLAM cell fractions based on PU.1 level.** (A) Experimental design for analysis of Myc levels in PU.1<sup>hi</sup> SLAM cells. (B) Representative FACS plot (left) and quantification (right) of Myc levels in PU.1<sup>hi</sup> SLAM HSCs from PU.1-EYFP mice treated with or without IL-1β for 20 d (n = 4/group). Individual values are shown with bars representing means. Data are compiled from two independent experiments. (C-E) Quantification by Fluidigm qRT-PCR array of IL-1 target gene expression (C), lineage gene expression (D), and HSC gene expression (E) in PU.1<sup>lo</sup> and PU.1<sup>hi</sup> SLAM cells from PU.1-EYFP mice treated with or without IL-1β for 20 d (n = 8/group). Data are expressed as log<sub>10</sub> fold expression versus -IL-1β. Box represents upper and lower quartiles with line representing median value. Whiskers represent minimum and maximum values. Data are representative of two independent experiments. (F) Representative FACS plots (left) and quantification (right) of cell cycle distribution in PU.1<sup>lo</sup> SLAM cells from mice treated with or without IL-1β for 20 d (n = 3/group) using Ki-67 and DAPI. Data are compiled from two independent experiments. (G) Experimental design (left) and quantification (right) of cell cycle distribution in PU.1<sup>lo</sup> and PU.1<sup>hi</sup> SLAM cells from mice treated with or without IL-1β for 1 d (n = 4/group). Data are compiled from two independent experiments. (H) Quantification by Fluidigm qRT-PCR array of cell cycle and protein synthesis genes in PU.1<sup>lo</sup> and PU.1<sup>hi</sup> SLAM cells from PU.1-EYFP mice treated with or without IL-1β for 1 d (n = 8/group). Data are expressed as log<sub>10</sub> fold expression versus -IL-1β. Box represents upper and lower quartiles with line representing median value. Whiskers represent minimum and maximum values. Data are representative of two independent experiments. (I) Quantification of fold change (f.c.) in geometric MFI of HSC<sup>LT</sup> from PU.1-EYFP mice treated with or without IL-1β for 1 d (n = 5/group). Individual values are shown with bars representing mean values. Data are representative of two independent experiments. \*, P < 0.05; \*\*, P < 0.01; \*\*\*, P < 0.001 by Mann-Whitney U test or ANOVA with Tukey's test in C-E, and H. Error bars represent SD.

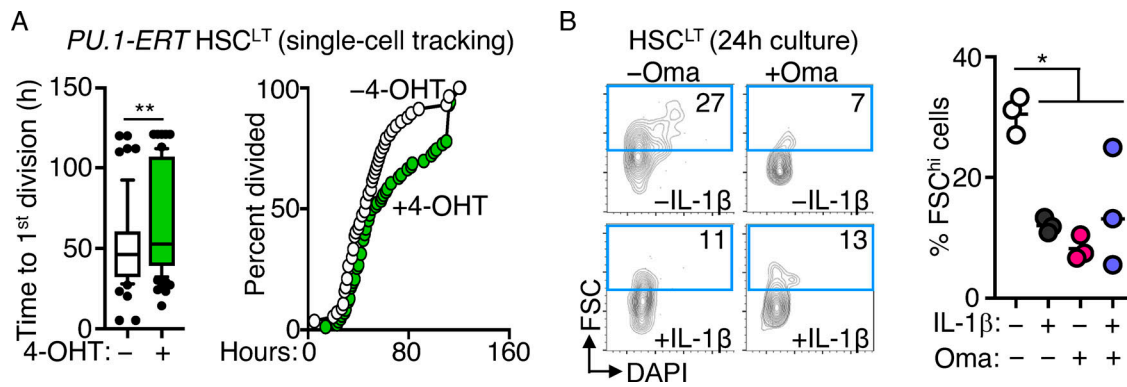
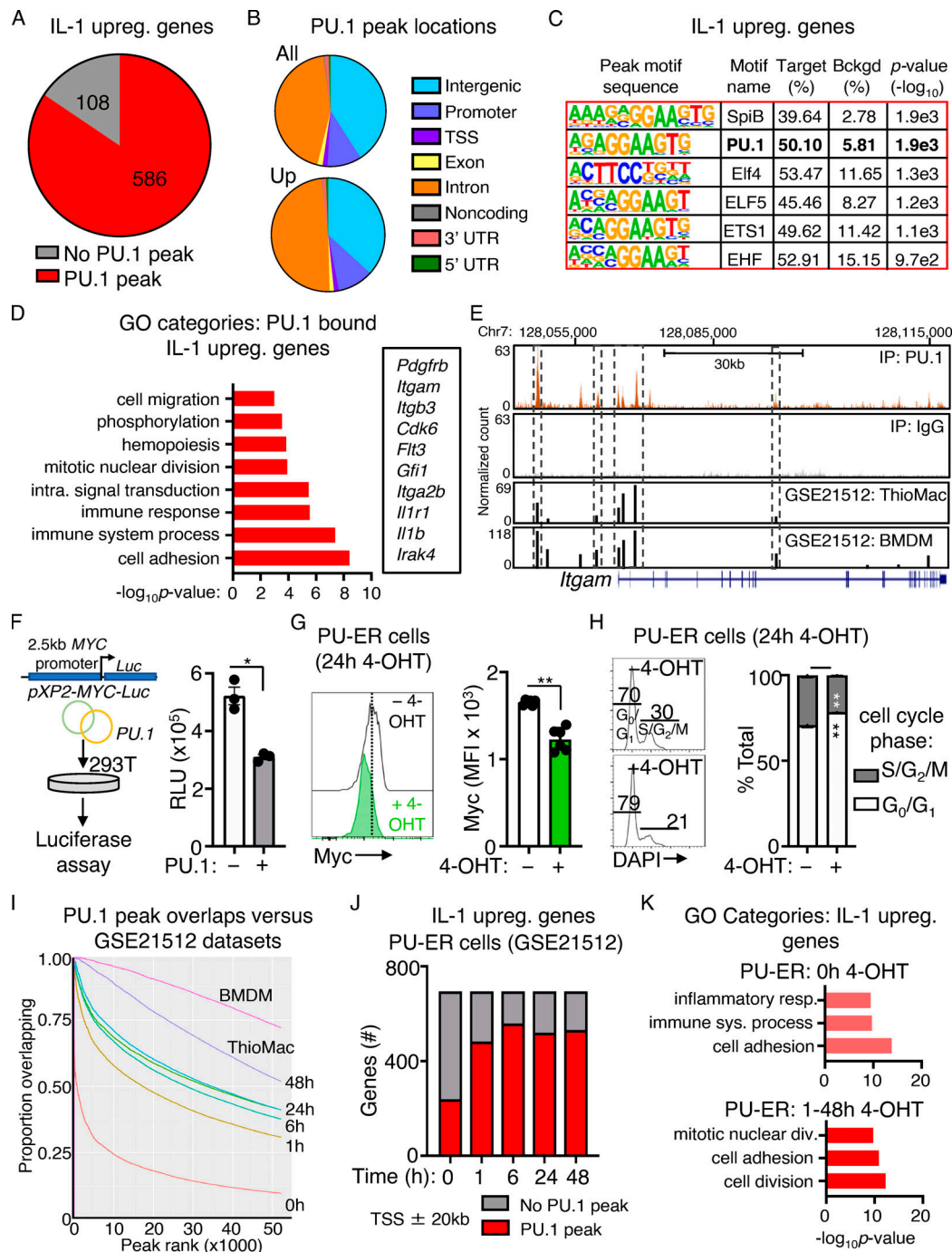
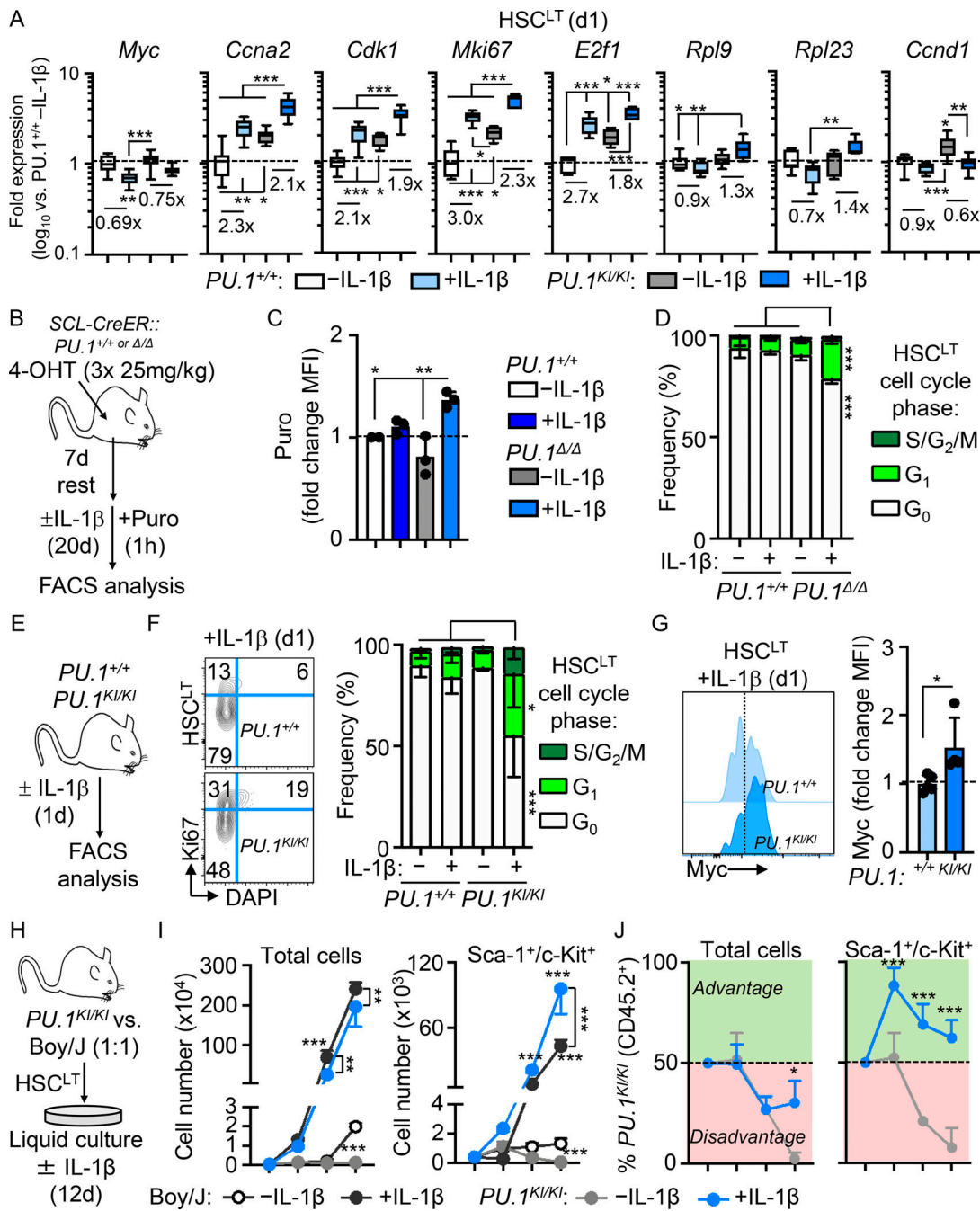


Figure S3. **Impact of PU.1 expression and Oma on HSC<sup>LT</sup>.** (A) Single-cell tracking studies of *PU-ERT* HSC<sup>LT</sup> cultured with or without 4-OHT. Quantification (left) of time to first cell division ( $n = 57$  -4-OHT; 86 +4-OHT) and graph showing kinetics of first cell division in HSC<sup>LT</sup> (right). Data are representative of two independent experiments. Box shows upper and lower quartiles with line showing median value, and whiskers upper and lower 10th percentile and individual dots represent outliers. (B) Representative FACS plots (left) and quantification (right) of FSC<sup>hi</sup> HSCs based on FSC/DAPI in HSC<sup>LT</sup> treated in vitro with or without IL-1 $\beta$  or with or without Oma for 24 h. Individual values are shown with lines representing mean values. Data are representative of two independent experiments. \*,  $P < 0.05$ ; \*\*,  $P < 0.01$  by Mann-Whitney  $U$  test or ANOVA with Tukey's test in B. Error bars represent SD.



**Figure S4. PU.1 binding to IL-1-upregulated genes and analysis of PU-ER cells.** (A) Pie chart comparing IL-1-upregulated genes identified in SLAM cells by RNA-seq analysis in Fig. 1 D and presence of PU.1 peaks at or near these genes (TSS  $\pm$  20 kb) in ChIP-seq data. See also Table S4. (B) Pie chart showing proportion of PU.1 peak locations in all genes versus IL-1-upregulated genes. (C) Transcription factor binding site motif enrichment at PU.1 ChIP-seq peak sites located at TSS  $\pm$  20 kb in IL-1-downregulated genes. (D) GO category enrichment of IL-1-upregulated DEGs containing PU.1 peaks. Representative genes in the indicated categories are shown to the right. Data are expressed as  $-\log_{10}$  P value. See also Table S5. (E) UCSC genome browser rendering of PU.1 peak location in *Itgam* gene body. Tracks show PU.1 ChIP-seq, WCE control, and peak locations and intensities in thioglycollate-elicited primary mouse macrophage (ThioMac) and BM-derived macrophage (BMDM) PU.1 ChIP-seq datasets from GSE21512. (F) Luciferase reporter assay measuring MYC promoter activity in 293T cells with or without PU.1 ( $n = 3$ /group). Data are representative of two independent experiments. (G) Quantification of Myc protein expression in PU-ER cells after 24 h culture with or without 4-OHT ( $n = 6$ /group). Data are representative of two independent experiments. Individual values are shown with bars representing mean values. (H) Cell cycle activity in PU-ER cells after 24 h culture with or without 4-OHT ( $n = 6$ /group). Data are representative of two independent experiments. (I) Comparison of PU.1 peak overlaps between PU.1 ChIP-seq data in A and datasets from GSE21512. (J) Comparison of IL-1-upregulated genes in SLAM HSCs with genes containing PU.1 peaks within TSS  $\pm$  20 kb in PU-ER cells with or without 4-OHT. Based on PU.1 ChIP-seq datasets in GSE21512. (K) GO category enrichment of IL-1-downregulated DEGs containing PU.1 peaks in PU-ER cell ChIP-seq dataset at 0 h with 4-OHT versus combined 1–48 h with 4-OHT. The top three GO categories are shown. Data are expressed as  $-\log_{10}$  P value. \*,  $P < 0.05$ ; \*\*,  $P < 0.01$  by Mann-Whitney U test or ANOVA with Tukey’s test in H. Error bars represent SD.





**Figure S5. PU.1 conditional knockout analysis and culture of PU.1<sup>KI/KI</sup> HSC<sup>LT</sup>.** (A) Quantification by Fluidigm qRT-PCR array of cell cycle and protein synthesis gene expression in HSC<sup>LT</sup> from mice treated with or without IL-1β for 1 d (n = 8/group). Data are expressed as log<sub>10</sub> fold expression versus -IL-1β. Box represents upper and lower quartiles with line representing median value. Whiskers represent minimum and maximum values. Data are from one experiment. (B) Study design for Cre induction with 4-OHT and analysis of HSC<sup>LT</sup> from SCL-CreERT PU.1<sup>+/+</sup> and PU.1<sup>Δ/Δ</sup> mice treated with or without IL-1β for 20 d (n = 2-3/group). (C) Intracellular flow cytometry analysis of puro incorporation in HSC<sup>LT</sup> from mice in E. Puro was injected i.p. 1 h before BM harvest. Data are expressed as fold change of MFI versus -IL-1β. Individual values are shown with bars representing mean values. Data are representative of two independent experiments. (D) Quantification of cell cycle phase distribution in HSC<sup>LT</sup> from PU.1<sup>+/+</sup> and PU.1<sup>Δ/Δ</sup> mice in B based on Ki-67 and DAPI. Data are representative of two independent experiments. (E) Experimental design for analysis of HSC<sup>LT</sup> from PU.1<sup>+/+</sup> and PU.1<sup>KI/KI</sup> mice treated with or without IL-1β for 1 d. (F) Representative FACS plots (left) and quantification (right) of cell cycle phase distribution in HSC<sup>LT</sup> from mice in H based on Ki-67 and DAPI (n = 7-8/group). Data are compiled from two experiments. (G) Myc levels from PU.1<sup>+/+</sup> and PU.1<sup>KI/KI</sup> mice treated with IL-1β for 1 d (n = 4-5/group). Individual values are shown with bars representing mean values. Data are compiled from two experiments. (H) Experimental design for competitive in vitro assays on Boy/J and PU.1<sup>KI/KI</sup> HSC<sup>LT</sup> cultured in a 1:1 ratio with or without IL-1β for 12 d. (I) Quantification of total cells (left) and immature Sca-1<sup>+</sup>/c-Kit<sup>+</sup> progenitors at the indicated time points (n = 3/group). (J) Quantification of frequency of total (left) and immature (right) CD45.2<sup>+</sup> cells derived from PU.1<sup>KI/KI</sup> HSC<sup>LT</sup> cultured with or without IL-1β at the indicated time points. Percentages >50 (color coded green in the graphs) are indicative of a competitive advantage for PU.1<sup>KI/KI</sup> cells. Data are representative of two independent experiments. \*, P < 0.05; \*\*, P < 0.01; \*\*\*, P < 0.001 by Mann-Whitney U test in G or ANOVA with Tukey's test. Error bars represent SD.

Six tables are provided online. Table S1 displays DEGs in SLAM cells from mice treated with or without IL-1 $\beta$  for 20 d. Table S2 provides an analysis of DEGs, with GO categories, IPA upstream regulator categories, and GSEA enrichment analysis of DEGs in SLAM cells from mice treated with or without IL-1 $\beta$  for 20 d. Table S3 shows a comparison of DEGs with public data, with overlap between IL-1–downregulated genes and public datasets. Table S4 displays PU.1 ChIP-seq peak locations, scores, and PU.1/Myc motif scores. Table S5 provides an analysis of PU.1 target genes, with GO categories enriched in IL-1 DEGs containing PU.1 ChIP-seq peaks. Table S6 lists the antibodies, antibody dilutions, and Fluidigm qRT-PCR primers used in this study.